DOE/JPL 956312/15
Distribution Category UC-63

Mobil Solar Energy Corporation
16 Hickory Drive
Waltham, Massachusetts 02254

STRESS AND EFFICIENCY STUDIES IN EFG

Program Manager: Juris P. Kalejs

Final Report – Subcontract No. 956312

Covering Period: July 9, 1982 – July 15, 1986

Distribution Date: July 15, 1986

Mobil Solar Energy Corporation
16 Hickory Drive
Waltham, Massachusetts 02254

STRESS AND EFFICIENCY STUDIES IN EFG

Program Manager: Juris P. Kalejs

Final Report - Subcontract No. 956312

Covering Period: July 9, 1982 - July 15, 1986

Distribution Date: July 15, 1986

ACKNOWLEDGMENTS

ABSTRACT

The goals of this program have been: (1) to define minimum stress configurations for silicon sheet growth at high ($\geq$ 3 cm/min) speeds; (2) to quantify dislocation electrical activity and their limits on minority carrier diffusion length in deformed silicon; and (3) to study reasons for degradation of lifetime with increases in doping level in EFG material. Among the main accomplishments have been:

(i) Development of a finite element model for calculating residual stress with plastic deformation (with Professor J. Hutchinson at Harvard University);

(ii) Verification of a finite element model for EFG control variable relationships to temperature field of the sheet to permit prediction of profiles and stresses encountered in EFG systems (with Professor R.A. Brown, MIT);

(iii) Development of residual stress measurement technique for finite size EFG material blanks using shadow Moiré interferometry (with Professor S. Danyluk, University of Illinois at Chicago;

(iv) Investigation of transient creep response of silicon in the temperature range between 800 and 1400°C in strain (10^{-3}) and strain rate (10^{-4} s^{-1}) regimes of interest in the stress analysis of sheet growth (at Mobil Solar);

(v) Establishment of quantitative relationships between minority carrier diffusion length and dislocation densities using Electron Beam Induced Current (EBIC) measurements in FZ silicon deformed in four-point bending in the temperature region between 800 and 1400°C (at Mobil Solar);

(vi) Quantitative characterization of the effect of boron and gallium dopants on bulk lifetime and on recombination around dislocations for EFG material.

The modeling work was supported by experiments carried out on EFG ribbon systems at Mobil Solar, which have studied the effects of post-growth temperature profile changes on ribbon stress and dislocation levels. Residual stress and dislocation densities were reduced by lowering growth speed to the order of 1 cm/min. At 2 cm/min and above, interface region temperature gradients had to be maintained at high values to maintain viable (stable) growth, and this has precluded obtaining such reductions. Stress analysis has shown that reduction of residual stress can be achieved by manipulation of transverse isotherms away from the growth interface, viz., cooling the sheet edge with respect to the center at distances of 1 to 5 cm from the interface. This is not effective in reducing high stresses very near (1 to 5 mm) the interface. The implication is that all vertical silicon sheet buckle-free growth may be creep limited at speeds in the range of 3 cm/min.

TABLE OF CONTENTS

LIST OF FIGURES

I. INTRODUCTION

A program to study stress generation mechanisms in silicon sheet growth was started at Mobil Solar on July 9, 1982. The purpose of the research was to define post-growth temperature profiles for the sheet that can minimize its stress during growth at high speeds, e.g., greater than 3 cm/min. The initial tasks were to develop computing capabilities to (i) model stress-temperature relationships in steady-state ribbon growth, and (ii) provide a means to calculate realistic temperature fields in ribbon, given growth system component temperatures as boundary conditions.

A computer code which accounted for plastic deformation effects on stress was generated at Harvard University, while a modeling capability to predict temperature profiles in EFG ribbon under realistic growth conditions was developed at Mobil Solar. The latter involved experimental work also, to develop a fiber optics-based thermometer.

The study of creep response of silicon above 1000°C and up to near the melting temperature was initiated in January 1983, when it was found that available data on the constitutive law were inadequate and did not apply for conditions relevant to plastic deformation in silicon sheet growth. First three-point bending, and then four-point bending apparatus was constructed and used to examine primary (transient) creep behavior of silicon for very short (less than 10 seconds) times under stress, which could generate up to $10^7/cm^2$ dislocation densities.

New subtasks in support of the stress analysis work were initiated at MIT and at the University of Illinois (Chicago) in April of 1983. Improved schemes for calculating growth system temperature distributions and for obtaining information on growth dynamics, so that real system behavior could be better understood, were developed using existing finite element models at MIT. The University of Illinois work examined the feasibility of using laser interferometric techniques to measure residual stress distributions in silicon sheet. Only average residual stress values obtained from a "scribe-and-split" technique were available and these were not useful for evaluating the detailed stress distributions predicted by the finite element models developed at Harvard.

1

Attempts to verify certain aspects of the stress modeling
met with limited success in study of high speed sheet growth
(3 to 4 cm/min) in the 10 cm EFG cartridge system because of the
complexity of the growth interface environment and of the nature
of the reheat region of the temperature profile in the
afterheater. A lower growth speed system for 5 cm wide ribbon
was constructed at Mobil Solar in early 1984, which provided a
very simple monotonically decreasing post-growth cooling profile,
and flexibility to manipulate it.

A task to develop Electron Beam Induced Current (EBIC) to
provide quantitative information on the electrical activity of
dislocations and their contribution to bulk diffusion length
degradation was started at Mobil Solar in April 1984, in a
significant redirection of the program. This subtask was
expanded in the continuation contract in July, and study of the
effects of dopants on degradation of the quality of low
resistivity EFG material was also initiated then. The new
emphasis on the characterization of the electrical activity of
defects was maintained throughout the remainder of the program
with extended studies of stressed silicon materials.

The final subtask in the program has examined a new approach
to the study of creep phenomena in silicon in the temperature
region from 800°C and 1200°C, where creep limitations are
suspected to strongly impact on residual stress. An apparatus to
measure stress relaxation, viz., the decay of stress applied at a
fixed strain (sample displacement), has been built and was used
to obtain data on silicon at Mobil Solar.

The following sections of this report summarize the main
results obtained in the various subtasks of this program.

II. SUMMARIES OF PROGRAM ACTIVITIES

A. Advanced System Design

At the time of initiation of this program, a satisfactory model that could account for stresses generated in silicon sheet growth at high speeds was not available. Numerous attempts to account for residual stresses suffered inadequacies in one area or another. The most prominent of these were the lack of a fully two-dimensional treatment of stress and temperature fields in the sheet width dimension, and the omission of plastic deformation effects. Two significant *factors preventing the development of* such a model were the absence of adequate information on creep behavior of silicon at high temperatures that could be applicable to the sheet growth situation, and of experimental data on temperature fields and deformation modes of growing sheet that could guide *the modeling effort.*

The work initiated under this subcontract attempted to develop and test in the laboratory a stress-temperature field model for EFG silicon ribbon that could overcome the above deficiencies. In the subtask at Harvard, a computer code to predict stress-temperature field relationships in steady-state sheet growth was developed. The stress state is parameterized by a two-dimensional temperature field and growth speed. Time dependent stress relaxation effects were incorporated through a creep law to model the impact of plastic flow on the sheet residual stress state.

A second aspect of this subtask dealt with development of a model to predict the temperature field in a moving sheet from given system component temperatures (i.e., the sheet environment) and study experimental means to verify it. A computer program was

3

developed at Mobil Solar to calculate sheet temperatures for given temperature boundary conditions in an enclosure surrounding the sheet. Several approaches to measure temperature profiles in the sheet under actual growth conditions were also developed. Thermocouples were used as well as a more sophisticated thermometer using fiber optics. When it was found that the 10 cm EFG cartridge system initially modeled generally was too complex to study basic phenomena and lacked the flexibility to allow various temperature measurements to be made, a simpler EFG system for 5 cm wide ribbon was designed and constructed to test various aspects of the stress and temperature field analyses.

Finite element techniques developed at MIT for solution of coupled capillary, heat and mass transfer equations in the EFG system also were applied to study the 10 cm cartridge system. These were able to predict sheet temperature profiles, present under actual growth conditions, which could be used in the stress analysis and in system optimization for combined growth stability and minimum stress. These calculations included extension of the finite element model to include fluid flow and dopant segregation in the meniscus so that the number of adjustable parameters could be reduced. The predictions of the model were compared, for the case of aluminum segregation, to experimentally deduced results for 10 cm cartridge operation with very good results.

The other subtask of stress model testing involved study of the high temperature creep behavior of silicon at high temperatures under conditions relevant to high speed silicon sheet growth. Three- and four-point bending apparatus was constructed and tested at Mobil Solar, and used to obtain data on various silicon materials: FZ wafers, high and low carbon concentration CZ silicon, EFG and dendritic web silicon sheets.

The major accomplishments in these areas of activity are described in more detail in the following subsections.

1. <u>Stress Analysis</u> (J. Lambropoulos, P. Mataga, and J. Hutchinson, Harvard University)

The method of analyzing steady-state growth of silicon sheet is covered in detail in an earlier report [1], and in the paper cited in the Appendix (Ref. [4]). The stress calculations subsequently have led to a closer examination and to progress in understanding of several very important issues associated with stress generating mechanisms in sheet growth. Only qualitative predictions using the stress model are possible even at this time, however, because of inadequate information on the creep law appropriate to sheet growth. A new approach to obtain data on creep response of silicon between 800°C and 1200°C was implemented in the latter stages of this contract (see Section A2 below), but interpretation of this data has not been completed to improve this situation at this time.

The extent to which stresses are reduced by creep was found to be very sensitive to the details of the temperature profile in the sheet as well as to the form of the creep law. A weaker dependence of residual stress on growth speed than anticipated on the basis of experimental results for the 10 cm EFG cartridge system was also found, and suggests that inadequacy of the creep representation at very high temperatures ($\geq$ 1200°C) may be responsible.

Attention was also focused on the appropriate stress boundary condition for sheet growth that is to be imposed at the liquid-solid interface. We have used a boundary condition for the stress component σ_{yy} (y is transverse coordinate in sheet width dimension) that $\sigma_{yy} = 0$ at the interface X = 0. The mathematics of the steady-state growth process is such that any initial distribution $\sigma_{yy}(y)$ at X = 0 can be prescribed. The choice of $\sigma_{yy} = 0$ at X = 0 is different from that used in stress analysis by other authors who have attempted to calculate stress distributions in silicon sheet growth using thermoelastic <u>static</u> theory. These attempts generally use a very large <u>non-zero</u> σ_{yy} at the solid-liquid interface in the analysis. We feel that this is not physical because such σ_{yy} values are orders of magnitude above the yield and flow stresses of silicon

5

over a considerable temperature range, and thus undoubtedly lead to wrong stress distributions in the case of steady-state growth, and cannot predict residual stress distributions.

The question of the appropriate interface boundary condition to use in the model developed here still remains an outstanding issue at this time. A simplified model governing the behavior of the stresses very near the interface was proposed [2] and showed that stress distributions obtained from the present model at distances greater than about 1 mm from the interface are independent of the interface stress, provided high creep intensities prevail.

When primary creep rate studies (see below) and new data on steady-state creep response of silicon above 1000°C became available more recently, as summarized in Table I, it was clear that the initial stress analysis had employed a constitutive law that considerably underestimated the creep intensity for sheet growth. Thus, more detailed calculations of stress in experimental systems were consequently carried out with creep laws a factor of up to 10^4 greater than originally envisioned. Predicted residual stress levels were accordingly reduced from unphysical levels of the order of 100 MPa maximum, which would buckle and even lead to fracture of ribbon at room temperatures, to levels of the order of 10 to 30 MPa more typically expected on the basis of experimental results. It appears that the highest steady-state representation, or "ultra-high" creep condition in Table I is perhaps the best available estimate of creep relaxation in high speed silicon sheet growth at this time.

A new scheme for calculating residual stress from residual inelastic strain was also developed [3]. This has introduced the concept of "misfit" strain and is related to a small but perhaps significant inhomogeneity in the velocity profile of the advancing liquid-solid interface across the growing sheet width. The misfit strain contribution to the total residual inelastic strain can be comparable to the creep contribution.

TABLE I

HIGH TEMPERATURE CREEP LAWS USED IN MODELING

$$\dot{\epsilon}_{ij} = C[\exp(-\beta/T)/T] \, (\sigma_e/\mu)^{n-1} \, S_{ij}$$

Reference	C (K/GPa–s)	β (°K)	n	$\dot{\epsilon}$ (s^{-1})*
Myshlyaev et al. "Low Creep" Condition	1.05×10^{29}	59,760	5.0	1×10^{-8}
"High Creep" Condition	1.05×10^{31}	59,760	5.0	1×10^{-6}
Siethoff and Schröter	5.85×10^{22}	41,800	3.6	41×10^{-6}
"Ultra-High Creep" Condition	1.05×10^{33}	59,760	5.0	100×10^{-6}

*Calculated strain rate for $\tau/\mu = 10^{-3}$ and T = 1300°K, with pure shear ($\tau = \sigma_{12}$).

$$\sigma_e = \sqrt{(3/2) \, S_{ij} \, S_{ij}}$$

$$S_{ij} = \sigma_{ij} - 1/3 \, \sigma_{kk} \, \delta_{ij}$$

$\mu = 63.7$ GPa.

A number of sensitivity studies examining the impact of changing the post-growth cooling profile of the sheet on residual stress were carried out. The most significant results were obtained for the case where the transverse isotherm (in the sheet width or y dimension) shape was varied. Reductions in residual stress are predicted for the sheet edge cooled with respect to the centerline. Peak thermoelastic stresses usually increase, however, and appear to produce the enhanced driving force to activate the stronger creep necessary to reduce the residual stress. The extent of the reduction and residual stress redistribution are functions of the distance from the growth interface at which the maximum excursion in the transverse isotherm variation is imposed, and of the creep intensity.

For edge-centerline temperature differences of 100°C with the edge cooled, it is possible to achieve peak residual stress reductions of up to 30-40 percent for certain growth conditions. The residual stress reduction is not very sensitive to growth speed in the range from 1 to 3 cm/min, or to the details of the transverse isotherm shape. A complete description of the results of the modeling is reported in a reference given in Appendix I, where a paper prepared for the First International Symposium on Shaped Crystal Growth (SSCG-1), and submitted to the Journal of Crystal Growth, is cited (Ref. [6]).

The extent of the stress reduction which can be achieved with manipulation of the transverse isotherms is very sensitive to the form of the creep law used in the calculation. The creep behavior of silicon in the most critical range for these calculations, that between about 1200 down to 800°C where the creep quickly becomes a limiting factor in stress reduction even for the slower speed growth range of 1-3 cm/min examined, is not well understood for conditions relevant to the sheet growth situation. For this reason, equipment to measure stress relaxation in this region was constructed and used to obtain stress relaxation information.

The main conclusion of the stress analysis has been that the sheet maximum stresses, which usually occur at high temperatures within a few mm of the interface and are likely to be those causing buckling as

8

speed is raised above 3 cm/min, and the residual stresses are very sensitive to details of the creep and of the cooling temperature profile in the growing sheet. Very intense creep is predicted to be required to reduce the stresses from thermoelastic values, which would be sufficient to buckle and fracture the sheet, to the levels of the order of 1-20 MPa usually observed experimentally.

The temperature field modeling indicates that the material constants of silicon impose the most fundamental constraints on heat flow conditions that contribute to producing large interface values of the second derivative of the temperature profile, hence high potential buckling stresses, under conditions necessary to maintain high speed growth (i.e., very large interface gradients in excess of 1000°C/cm). This implies that all vertical buckle-free silicon sheet growth will be limited to the order of 3 cm/min, and that the "window" for obtaining low stress configurations even at slower speeds is severely constrained by the difficulty in manipulation of the temperature profile very near the growth interface without compromising growth speed capability. Moreover, it does not appear that the stress reductions predicted to occur from adjustment of transverse isotherm shapes can be made large enough to overcome the dominant effect of the axial profile curvature, although this may be useful in producing significant stress reductions within a lower growth speed range. Better representations of the creep law are required to obtain more quantitative information.

2. Experimental Aspects of Stress Generation (Mobil Solar)

The experimental work undertaken at Mobil Solar was directed mainly at support of the stress analysis effort described above: to generate information on creep that could be used to make the stress calculations more quantitative; to operate EFG ribbon systems to provide a place to test the practical aspects of the model predictions; and to develop modeling and experimental approaches to obtain information on the temperature distributions in a growing silicon sheet, extremely vital to making stress predictions for growth systems in practical use. The work in these three areas is summarized in what follows.

9

a. <u>Creep Law Studies</u> (A.A. Menna and M.P. Brodeur)

Constitutive relationships between the strain rate and stress for silicon usually have been derived on the basis of work hardening data taken between 1000 and 1300°C, and at larger strains and strain rates than typically encountered in silicon sheet growth. This situation is illustrated by reference to Fig. 1. The shaded region 1 of the stress-strain curve is that appropriate for sheet growth, with maximum strain and strain rates typically in the ranges of 10^{-6} to 10^{-4}, and 10^{-4} to 10^{-2} s^{-1}, respectively. Evidence of Lüders-like band formation was found in EFG ribbon cross sections, indicating that strain instabilities previously associated with larger strains, of the order of percent in the shaded region 2 of Fig. 1, were also triggered during sheet growth. The available creep data of Myshlaev et al. and Siethoff and Schröter summarized in Table I were taken at constant strain rates and large strains of the order of 10 percent, as represented by the shaded region 3 in Fig. 1. Dislocation densities produced in the latter are of the order of $10^8-10^9/cm^2$, as compared to average levels of $10^7/cm^2$ and below observed in EFG material.

Transient creep experiments were carried out at Mobil Solar in three- and four-point bending apparatus built especially to withstand operation up to the melting temperature of silicon, 1412°C. These were made from graphite, and built to closely conform to the ASTM (e.g., E328) standards. Some testing of as-grown EFG material was carried out, but its creep response was found to be very nonuniform because of grown-in structural inhomogeneities. Thus, most of the creep experiments were subsequently done with CZ silicon wafers of various carbon levels, and with FZ silicon. The temperature region between 1200°C and 1400°C, where data was not available, was chosen for study initially and later these creep studies were extended down to 700°C, where there was no more creep observed at the load of 5-20 MPa chosen for the study.
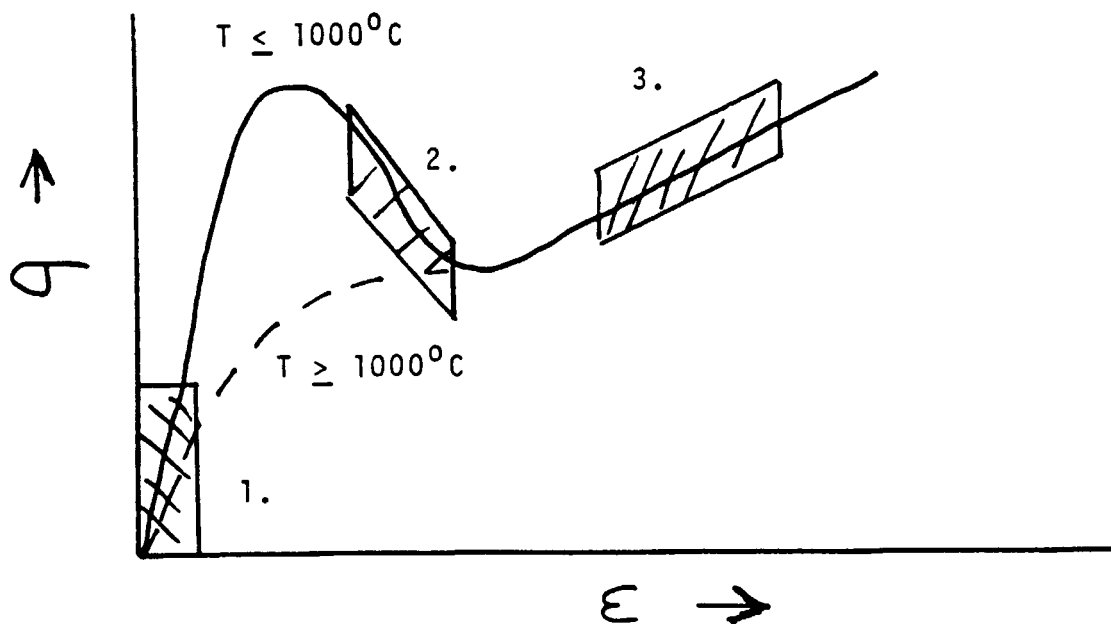
$T \leq 1000^\circ C$

$T \geq 1000^\circ C$

1. __Primary Creep - Present Work__

$$0 \leq \epsilon \leq 10^{-2} \quad , \quad 0 \leq \dot{\epsilon} \leq 10^{-3} \, s^{-1}$$

$$N_D \leq 5 \times 10^7 / cm^2$$

2. __Lüders Bands (Mahajan et al., Acta Met. 27(1979) 1165.)__

Observed for $T \leq 1000^\circ C$

3. __Secondary Creep - Steady-State__

$$\epsilon \geq 1 - 10\% \quad , \quad N_D \geq 10^8 / cm^2$$

Fig. 1. Stress-strain regimes for creep.

11

Near the conclusion of the contract, a stress relaxation apparatus was constructed to further explore the creep behavior of silicon in the temperature region between 800 and 1200°C which was found to be very critical for some aspects of the stress modeling studies. Rather than obtaining data of strain and strain rate changes at constant applied load, these measurements provide information on the relaxation rate of a load at constant strain, i.e., at fixed displacement amplitude.

It is to be expected that the generally complex structure of EFG silicon material, with its high density of twin bands and other non-uniformities in crystallite orientation and impurity content, responds very differently to applied loads than does the single crystal silicon wafers typically used in testing. Thus, one of the more significant initial findings of the four-point bending study was that the as-grown EFG material still has a very rapid creep response at 1050°C, as shown in the data of Fig. 2. These illustrate both the nonuniform response and the fact that a fast transient or primary creep response even in this work-hardened material is over in times of the order of one minute or less. This deformation was found to be permanent in that there was no subsequent elastic spring-back with load removal. These results guided further experimentation above 1000°C on single crystal material, where load application times and magnitudes were generally chosen to study the primary creep regime with load times of the order of 10 seconds or less.

In general, very little information on the creep response of silicon above 1200°C is available. Some of the present work conse-quently examined the very high temperature creep, as shown by the data in Fig. 3, and contrasted the relatively low impurity content FZ silicon to CZ silicon with high oxygen and carbon concentrations. Figure 4 shows cross-sectional micrographs of several of the FZ silicon samples stressed above 1375°C. Figure 4(a) gives the dislocation configuration for an undeflected FZ sample loaded to 1.4 MPa, heated up to about 1400°C under load, and held at temperature for 100 minutes. No deflection was measurable after cool-down. Figures 4(b) and (c) show the dislocation configurations after long and short times under stress
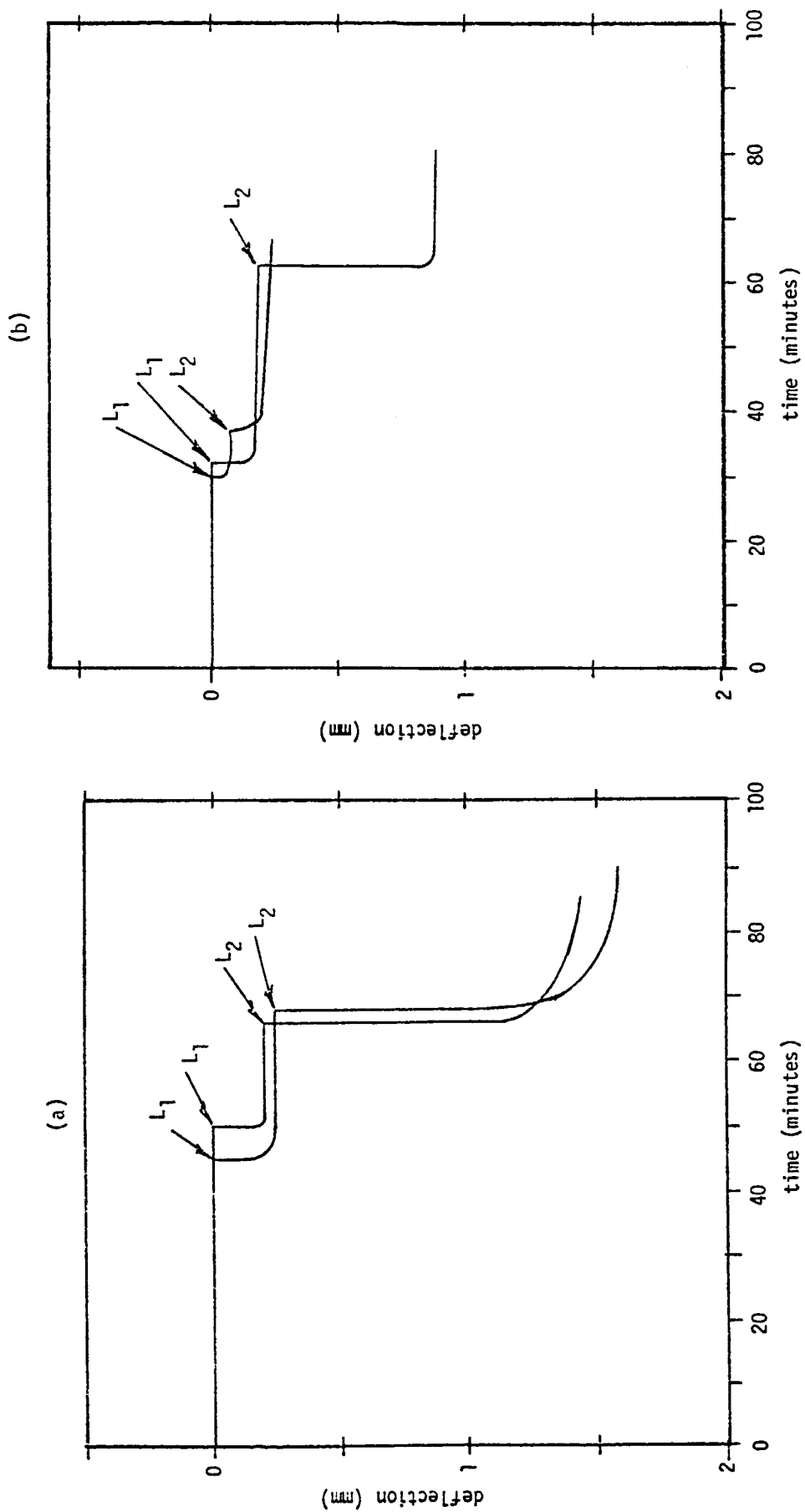
Fig. 2. Response of ribbon stressed in four-point bending at 1050°C under loads of L_1 = 170g and L_2 = 440g.
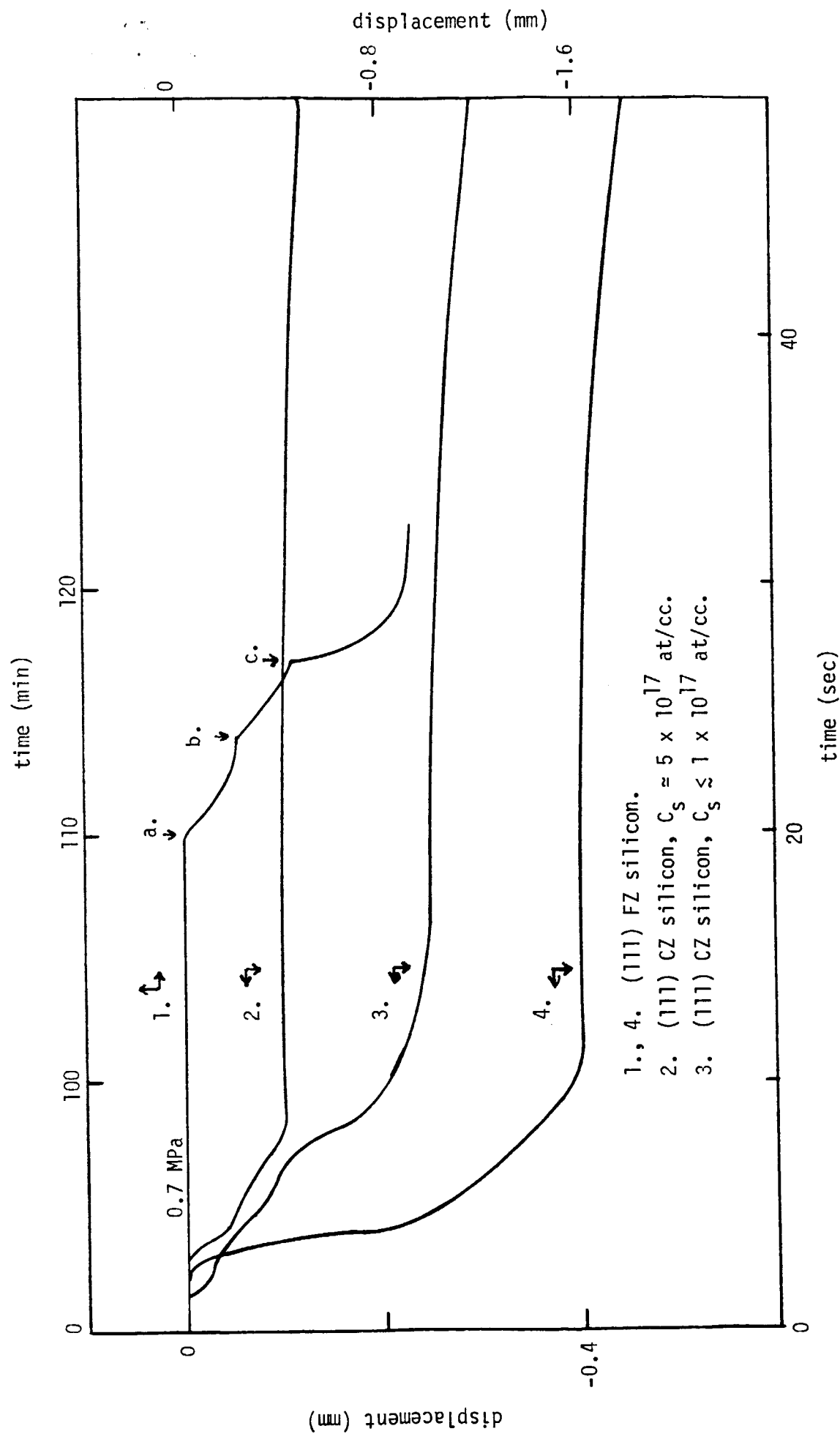
Fig. 3. High temperature, low stress creep response of several different silicon materials: 1. multiple loading for FZ with a. 3.5 MPa, b. 4.2 MPa, c. 5.0 MPa; see text for other details.

1., 4. (111) FZ silicon.
2. (111) CZ silicon, $C_s \approx 5 \times 10^{17}$ at/cc.
3. (111) CZ silicon, $C_s \lesssim 1 \times 10^{17}$ at/cc.
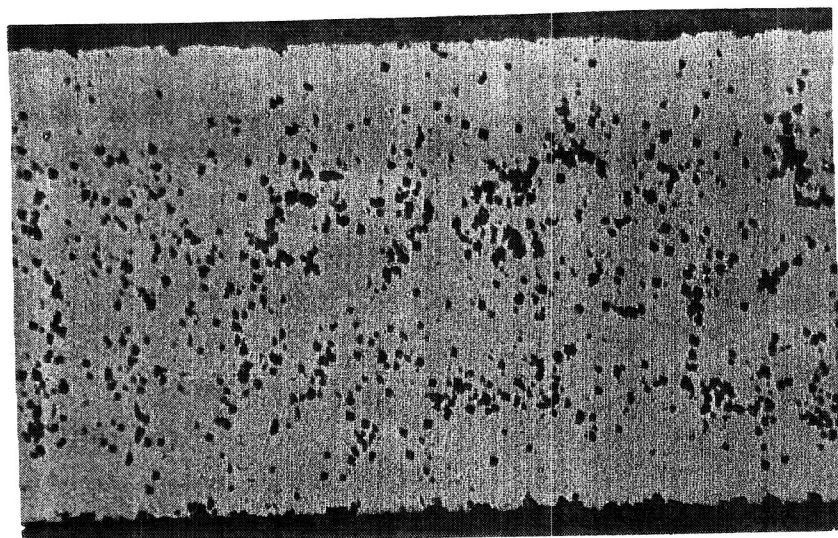
(a)
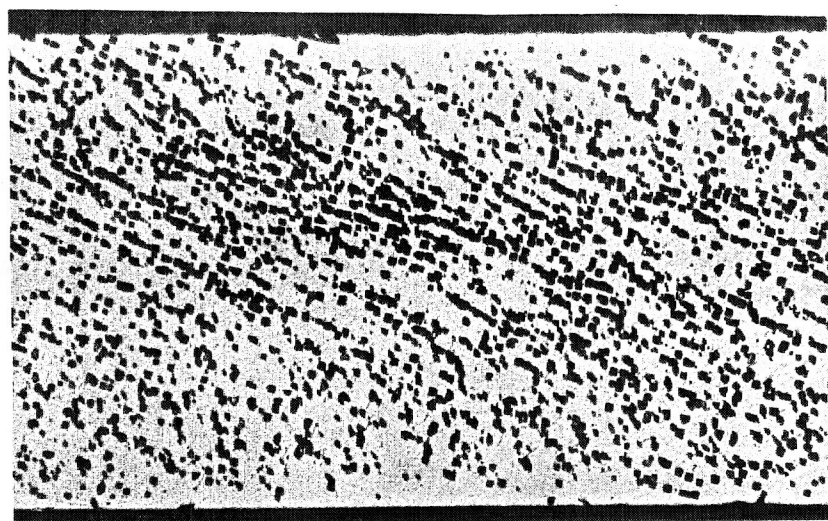
(c)
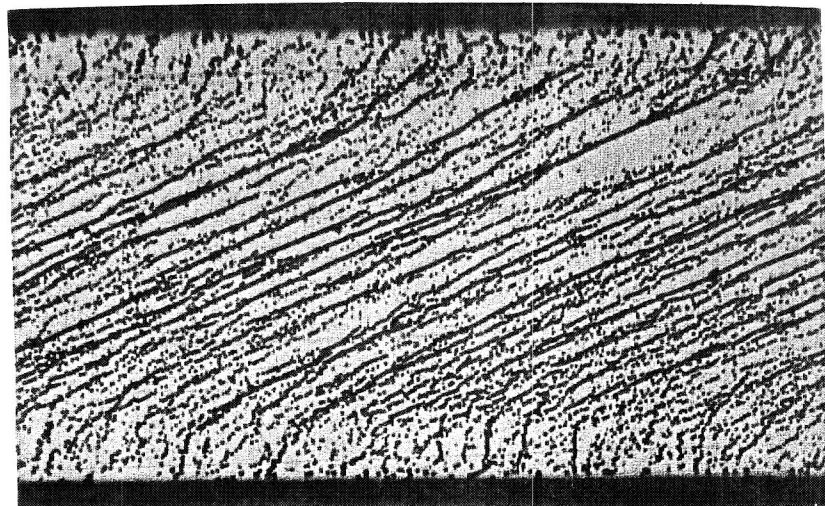
(b)

Fig. 4. (111) FZ silicon dislocation configurations after very high temperature (~1400°C) loading: (a) $N_D = 5.5 \times 10^5/cm^2$; (b) $N_D = 4.0 \times 10^6/cm^2$, and (c) $N_D = 1.1 \times 10^6/cm^2$. Compression surface at bottom (165X) and <110> bending axis. See text for details.

near 1400°C, as represented by curves 1 and 4 in Fig. 3, respectively. It appears that significant polygonization has occurred only for the case of the sample of 4(b) which was stressed under multiple loading conditions for 120 minutes at 1390°C. Curves 2 and 3 in Fig. 3 show the effect of oxygen and carbon on the creep response at 1375°C under conditions similar to curve 4 for the FZ silicon. A load of 5.0 MPa was used for all these samples. The carbon-rich CZ sample 2 appears to have a reduced creep response beyond that produced by the oxygen alone in sample 3.

Additional differences between the FZ and CZ silicon materials are illustrated by the more extensive data of Fig. 5, which also examines a higher stress range. Here, CZ and FZ silicon data at 1370°C and stresses between 7 and 16 MPa are compared, including a (100) surface CZ silicon sample. Again, the higher creep response in FZ silicon is evident from comparison of responses at comparable stress levels. The (100) CZ sample, with very low carbon but 1×10^{18} at/cc oxygen does not exhibit a qualitatively different strain rate from that of the FZ silicon at the highest stress levels of 15 MPa. However, there is considerable uncertainty with respect to resolution of the time scale at these short times, so further conclusions cannot be drawn. The higher carbon CZ (curves 2 and 3) does show some indication that the creep response remains reduced from that of FZ silicon even at higher loads. The maximum dislocation densities generated in these samples were typically $1-5 \times 10^7/cm^2$.

Four-point bending experiments were carried out at 1000°C and below to determine the extent of creep at lower temperatures. FZ silicon of (111) surface orientation and ⟨110⟩ bending axis was loaded at 600°C and 800°C for one hour at 25 MPa. No detectable deflection was observed in either case. Cross-sectional photomicrographs showed that no dislocations were introduced at 600°C. A low dislocation density was observed for the 800°C sample, with most dislocations concentrated around the load application points. The average dislocation density in the central, uniformly stressed region was lower. The dislocations were inhomogeneously nucleated, often along two principal (111) slip planes.

16
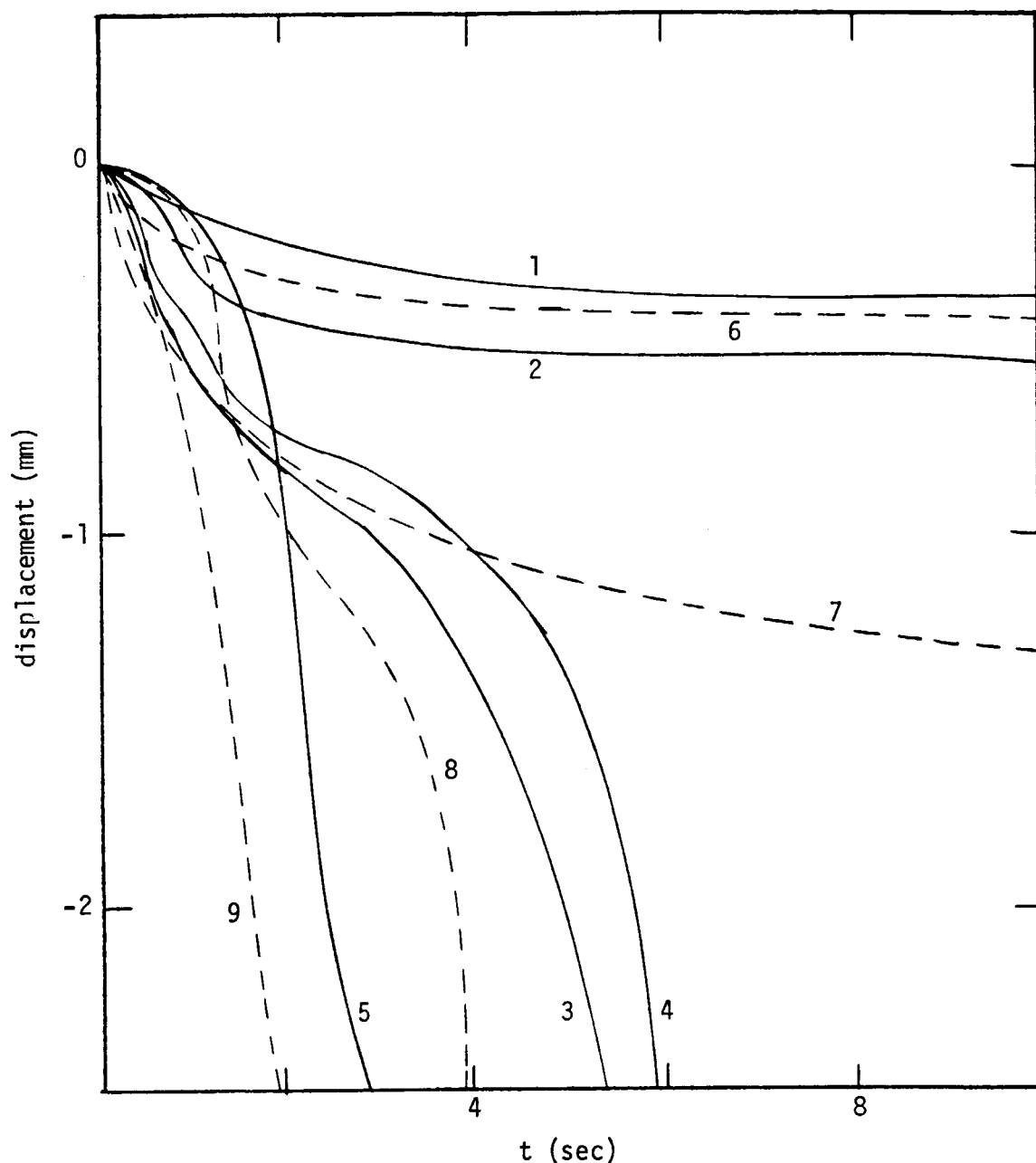
Fig. 5. Creep response of FZ and CZ silicon at 1370°C. <110> bending axis.

1. (111) CZ at 7.0 MPa $\quad C_s \simeq 5 \times 10^{17}$ at/cc
2. (111) CZ at 12.0 MPa $\quad C_s \simeq 5 \times 10^{17}$ at/cc
3. (111) CZ at 15.5 MPa $\quad C_s \simeq 5 \times 10^{17}$ at/cc
4. (111) CZ at 13.5 MPa $\quad C_s \simeq 1 \times 10^{18}$ at/cc
5. (100) CZ at 13.5 MPa $\quad C_s \lesssim 1 \times 10^{17}$ at/cc
6. (111) FZ at 8.0 MPa
7. (111) FZ at 12.0 MPa
8. (111) FZ at 14.0 MPa
9. (111) FZ at 15.5 MPa

17

FZ silicon as well as EFG ribbon and Westinghouse WEB were stressed at 1000°C. The latter was done to generate samples for Cornell University, who will study the material using TEM. Web samples with and without dendrites attached were stressed. The results are given in Fig. 6. A single EFG ribbon also was stressed. The FZ silicon used in the initial experiment (curve d) exhibited so much creep that it was bent to the maximum extent and fell out of the bending apparatus after about 100 seconds of loading. Thus, this line gives only an approximate displacement curve. Additional FZ silicon samples were then loaded for progressively increasing time intervals, as shown by the circles: 25 seconds, 50 seconds, 75 seconds, and finally 105 seconds (curve e). These samples have been also used in the electrical characterization subtask discussed below.

The main conclusion drawn from the above primary creep studies was that silicon above 1200°C can be treated as an essentially plastic solid insofar as its responses to stress above about the 5 MPa level are concerned. Attempts were made [5] to analyze the data using approximations that could give estimates of the creep law to within an order of magnitude. These led to a representation of the primary creep response of the form given in Table I, with a stress dependence $\dot{\varepsilon} \sim \sigma^{10}$ which is a very weak function of temperature not resolved within the limited scope of the data.

The constitutive law used in all the stress analysis described here is of the form deduced from the secondary creep data as represented in Table I. However, the experimental primary creep data strongly suggest that a reformulation of the stress analysis using a flow stress concept could lead to an improved representation of plastic deformation conditions occurring during crystal growth. However, the creep data is still too incomplete at this time to justify a reformulation that would replace the adjustable parameters used in Table I by new ones.

The temperature region between 800°C and 1200°C was found to be of particular concern in some of the later stress analyses involving transverse isotherm curvature effects, and thus a new approach to

18
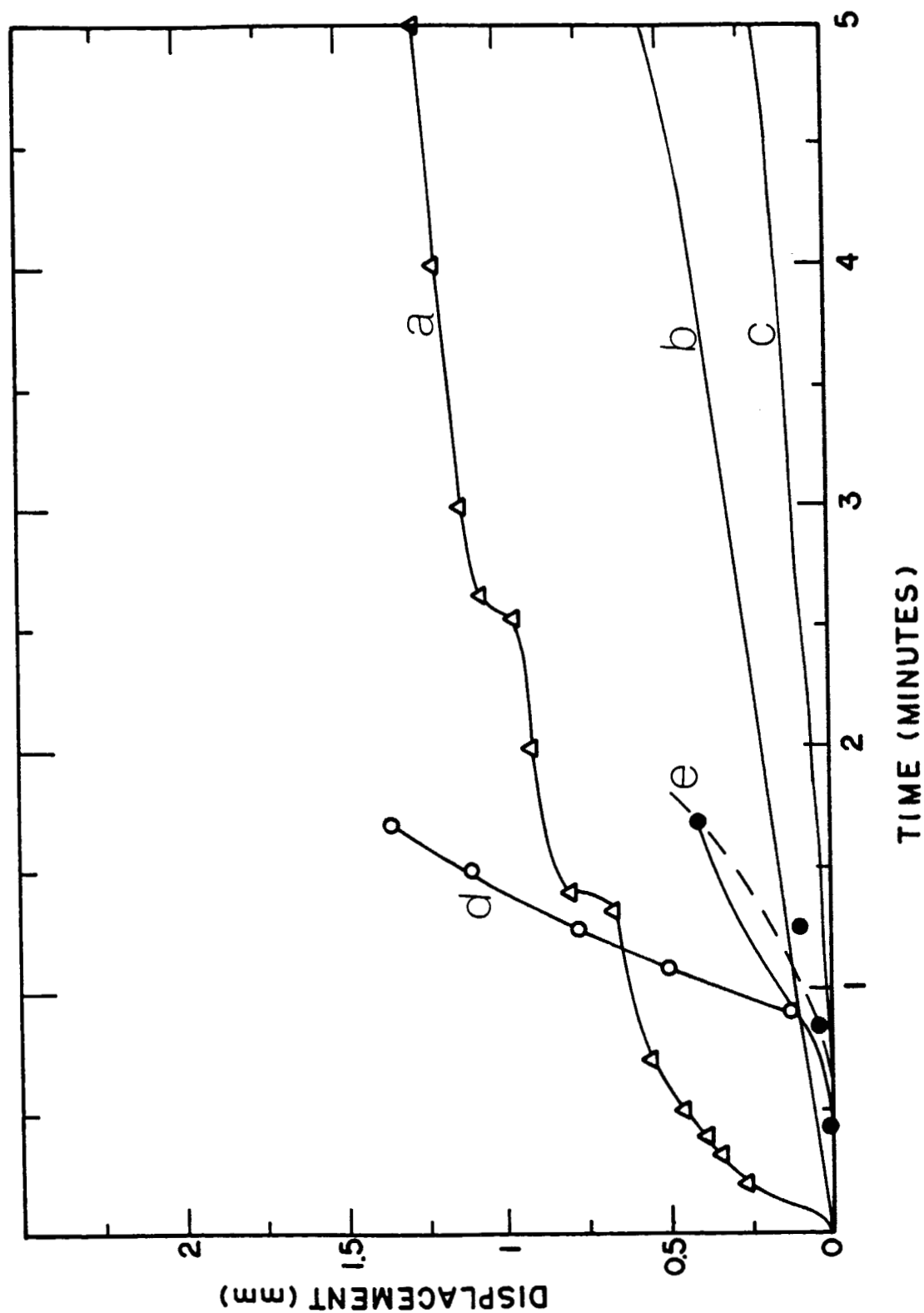
Fig. 6. Creep response of various types of silicon to four-point bending at 1000°C:
a) Westinghouse WEB at 25 MPa with dendrites removed; b) Westinghouse WEB
with dendrites at 25 MPa; c) EFG ribbon at 52 MPa; d,e) (111) FZ silicon at
25 MPa; the dashed line represents average behavior of samples loaded for
times of 25, 50, 75, and 105 seconds (solid circles) at 25 MPa.

obtaining constitutive law information there was started in the last
stages of this contract. This involved measurement of stress
relaxation at constant strain (sample displacement). A modified form
of the four-point bending apparatus was again used. Although initial
data have been obtained from these experiments, there was not time to
examine them thoroughly to obtain information for stress analysis
purposes before the termination of this contract. Details of this
work are found in Appendix III.

b. __EFG Ribbon Growth__ (A.A. Menna and M.P. Brodeur)

Several EFG ribbon systems were operated in this
program in order to provide experimental data in support for various
aspects of the stress analysis. Efforts first were made to obtain
detailed information on the ribbon temperature distribution
encountered under different growth conditions in a given system, and
with system afterheater region design modifications, as input data for
the stress analysis. The experimental efforts in measurement of
ribbon temperatures and associated finite element modeling of heat and
mass transport (see also Section c below) provided information that
allowed specification of ribbon temperature profiles with confidence
that they were representative of those present in the EFG systems
studied under actual operating conditions. However, efforts were not
successful in finding design modifications that produced lower stress
EFG material at high ($\geq$ 2 cm/min) speeds. More details of this work
are given next.

During the course of the program, two approaches to obtaining
information on temperature distributions in the growing sheet were
tried out. Conventional thermocouples were attached to strips of EFG
ribbon by drilling a hole in the ribbon and gluing in the thermocouple
tip with graphite paste. The thermocouple could then be easily
lowered through the growth system and maps of the temperature field
obtained. This technique provided useful information to within a few
mm of the interface, where the resolution set by the finite size
thermocouple bead limited the results. The second approach used a
thermometer based on fiber optics [2]. This method utilized optical

20

fibers of high quality as sensor elements. The aim was to design high resolution sensor tips, of the order of 10 mils diameter, which could provide information on a scale of the order of 0.25 mm, either through a contact or non-contact mode of measurement.

A schematic of the measurement system is shown in Fig. 7. Al_2O_3 was used for the high temperature region, SiO_2 at lower temperatures. Acceptable sensitivities (~4 mV/°C) were obtained in this way using a conventional photomultiplier tube. A two-wavelength measurement was employed, using filters at 0.6 and 0.7 μm. Calibration curves up to the melting point of silicon were obtained. However, some stability problems were encountered that appeared to be associated with probe tip degradation in the furnace. Also, there were difficulties in mounting the sensor in the complex growth system environment, and the sensor was not put into use when it was demonstrated that the conventional thermocouple measurements combined with quantitative modeling of the EFG growth systems provided acceptable temperature field information for the stress analysis.

In the search for low stress EFG process growth configurations, a number of modifications in afterheater design have been tested in Furnace 17, where ribbon has been grown at speeds from 0.6 to 1.0 cm/min. This slow growth speed range was chosen for several reasons. First, it was decided to attempt to search for parameters that would produce EFG ribbon with much lower dislocation densities and examine how these relate to the speed variable. Also, the simplified design of the EFG system in this case (removal of the cold shoe typically used to enhance growth speed) would be a benefit, both for simplifying the stress analysis and for interpretation of the results through replacement of a temperature profile with a reheat region by one that is monotonically decreasing. The dislocation density was used as the principal means to monitor progress in reducing stress, although initial measurements of sheet stress using the interferometric technique developed at the University of Illinois gave additional stress information in later phases of the work.

21

LOW T
FIBER

HIGH T
FIBER

LENS

FILTERS

PHOTO MULTIPLIER
TUBE CIRCUIT
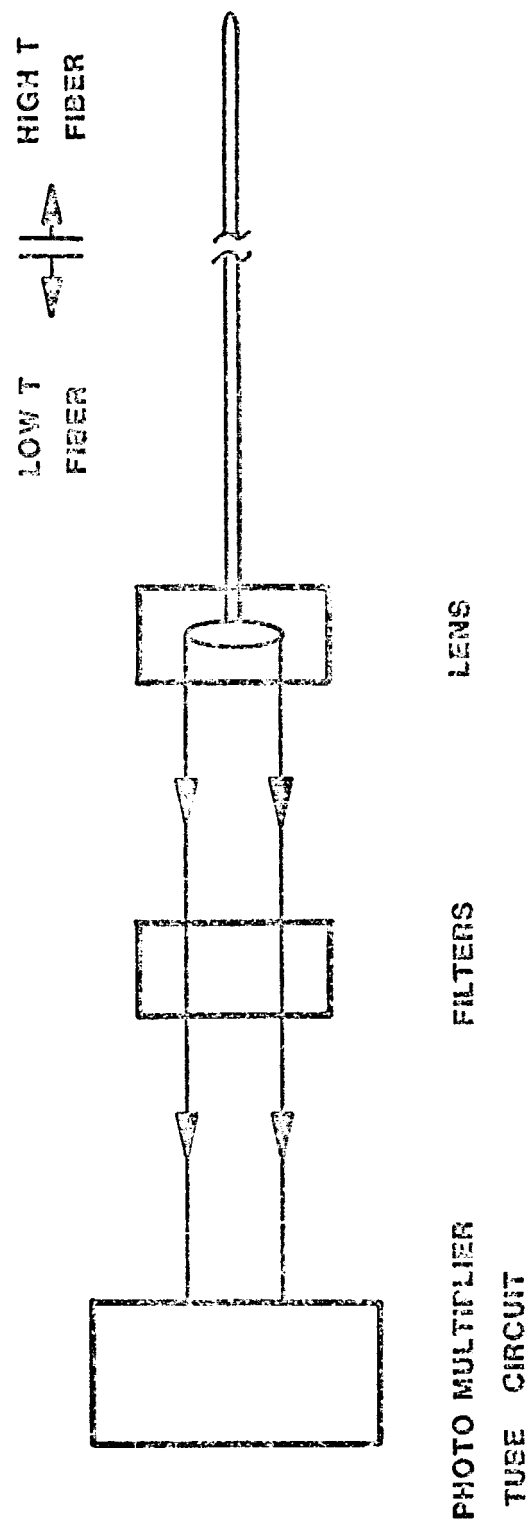
Fig. 7. Fiber optics temperature sensor schematic.

22

The main findings for the present growth mode were that the dislocation density is considerably reduced for the 5 cm wide ribbon grown below 1 cm/min from that in the more typical EFG material produced at 2 cm/min and above. The maximum densities were between 1×10^5 and 1×10^6/cm^2, down by about an order of magnitude. However, a considerably larger portion of the cross section was almost "dislocation free", i.e., densities in the range of 10^4/cm^2 and below, and there was evidence that Lüders band formation was significantly reduced. In several growth runs, the ribbon cross section showed no such highly dislocated regions at all.

It has not been possible to establish relationships between changes or further decreases in dislocation density and afterheater region design changes which were aimed at modifying the post-grown cooling profile below about 1000°C. Some ribbons have been of remarkably low dislocation density, but this has occurred rather randomly. This result appears to be tied more to contaminating impurity variations than to specific changes in cooling profile. Also, no significant variations in dislocation density with growth speed over the range 0.6 to 1.0 cm/min, or with dopant level were observed in this system.

The lower average dislocation densities for this ribbon are consistent with the results of residual stress measurements. These show among the lowest stresses observed in EFG material, with maximum values of 1-2 MPa, as compared with about 5-10 MPa in ribbon grown at 2 cm/min and above in other EFG systems.

It was concluded that a baseline threshold for dislocation densities of about 10^5/cm^2 is set in EFG material by interface region variables not consistently or easily controlled, and that operation in this slower growth speed range is most instrumental in reducing levels of dislocations by an order of magnitude from those typical in growth at 2 cm/min and above. The interface temperature gradient, which ultimately sets the speed capability of the system, is estimated to be still high, at about 1000°C/cm, from temperature profiling of the system using a ribbon with an attached thermocouple.

23

Even at this value, it is observed that there are limits in the range 1.2 to 1.4 cm/min on the maximum growth speed that can easily be sustained. This limitation arises mainly because of the need to control the ribbon ends, which are much thicker, and hence have lower temperature gradients. Thus, although it would be desirable to go to even lower temperature gradient growth, this practical limitation prevents it from being a viable approach in EFG ribbon systems in general.

c. Temperature Field Modeling (R.O. Bell, H.M. Ettouney)

Information on ribbon temperature distributions used for the stress analysis was obtained through the combination of two modeling schemes. A capability for predicting temperature profiles in a moving sheet from measured system component temperatures was developed at Mobil Solar [1]. This was successfully applied to model the 10 cm EFG cartridge system with cold shoes, and a second experimental EFG system for 5 cm wide ribbon constructed to examine aspects of afterheater design. Details of the modeling scheme were presented at a JPL Research Forum (see Ref. [3] in Appendix I).

The second approach utilized a finite element scheme developed at MIT (see Ref. [5] in Appendix I). The solutions of the coupled capillarity and heat and mass transfer equations were used to generate operating diagrams for process variables such as the sheet thickness, the growth speed, and the capillary rise height. These solutions were capable of predicting interface shapes in addition to the sheet temperature profiles. The interface shape and meniscus configurations were then used with complete solutions for the Navier-Stokes equations in the die and meniscus melts to study impurity segregation. Aluminum-doped 10 cm wide ribbon was grown under known conditions for this study. Together with experimental data on the thickness-velocity relationships, the segregation data allowed the model to be fit with only one adjustable parameter, the die temperature. The ribbon temperature profiles derived from these calculations were uncertain only to the extent of a lack of knowledge concerning the fundamental physical constants of silicon, e.g., the thermal conductivity, emissivity and the solid optical absorption coefficient. Additional details on this work can be found in Refs. [3] and [5] in Appendix I.

The models for the temperature field were applied to investigate several important effects, in the one case that of imposing transverse temperature field variations in a growth system [4], and in study of sheet stress sensitivity to dynamic growth condition changes and to the use of graybody and blackbody approximations to heat transfer [5].

B. Defect Electrical Characterization
(C.E. Dubé and D.B. Sandstrom)

This subtask on the study of electrical activity of defects in silicon using the electron beam induced current (EBIC) mode of the SEM was undertaken to quantify dislocation recombination and to study the manifestations of plastic deformation by comparing dislocations in deliberately stressed material and in EFG sheet. Initially, this required development of quantitative EBIC analysis techniques for measurement of minority carrier diffusion length at high resolutions in the neighborhood of the dislocation as well as throughout inhomogeneously dislocated areas. These techniques were then used to study dislocations in FZ and CZ silicon stressed in four-point bending throughout the temperature region from 800 to 1400°C and to compare the results to dislocation activity in as-grown EFG material. Details of this work are summarized below.

1. EBIC Mode Qualification (with J.I. Hanoka)

Reproducibility studies and calibration of the EBIC measurement of minority carrier diffusion length L_n were carried out on Schottky barriers in the low injection mode with electron beam currents as low as 10^{-11} amp and a carrier density of the order of $10^{13}/cm^{-3}$. A calibration scheme was set up to permit measurement of L_n with a high level of absolute accuracy by correlating the EBIC current I with L_n measured by an independent method, the infrared photovoltage method (IRPV) [6]. The relationship between the IRPV and EBIC values of L_n obtained from measurements on control samples is shown in Fig. 8. These samples were all free of extended defects and thus the measurement is not affected by sample inhomogeneity.

25

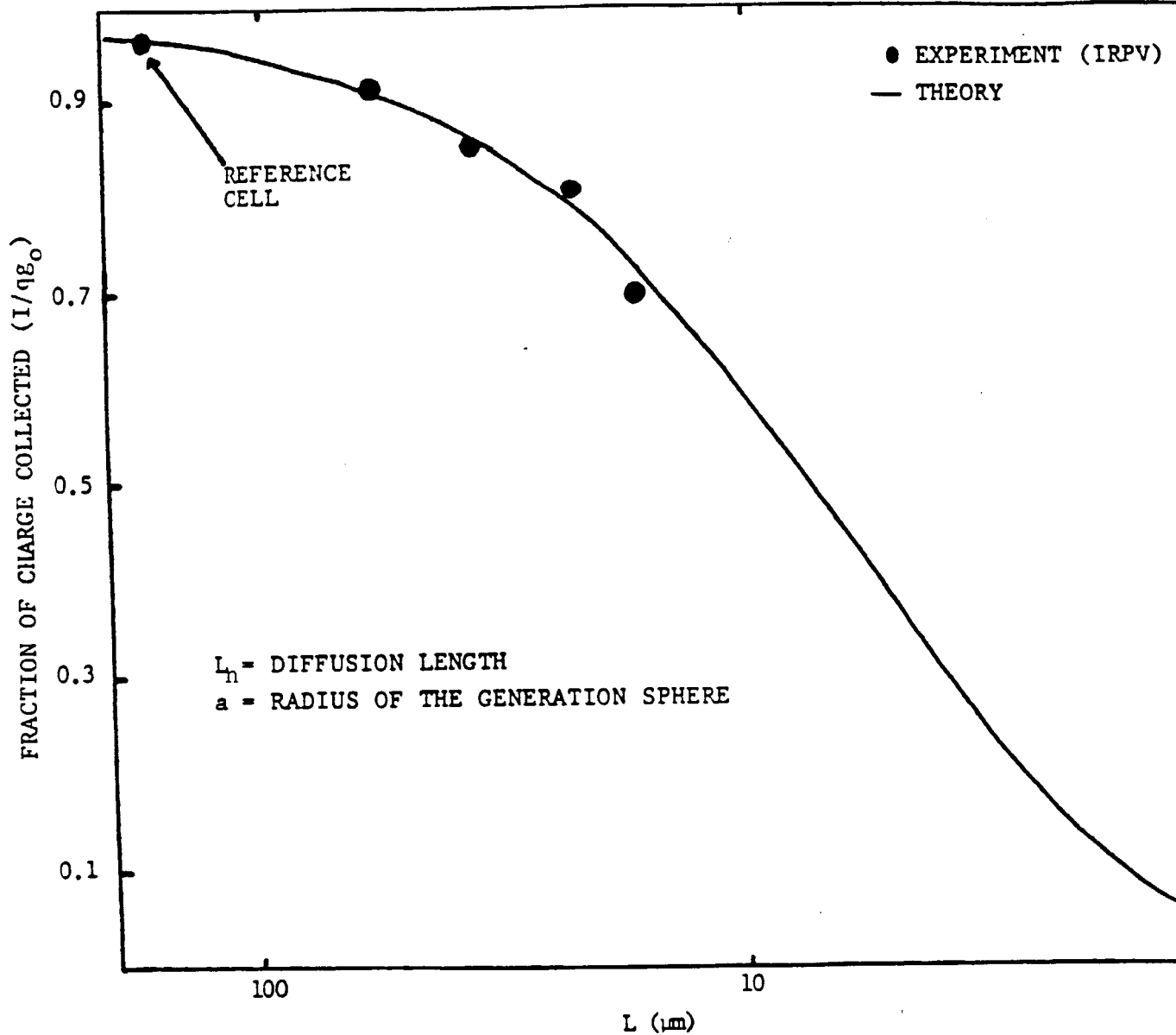$$I = 3qg_o\ (L/a)^3\ e^{-a/L}\ [a/L\ \cosh\ a/L - \sinh\ a/L]$$

Fig. 8. Plot of I/qg_o vs. L_n for a 40 keV beam. Also shown are results for experimentally measured I/qg_o and L_n. Here q is the electronic charge, g_o is a generation rate constant.

26

In order to allow quantitative measurements of L_n to be made in the sample cross section, the EBIC technique was extended to surface barriers fabricated on the edge of wafers typically 300-400 μm in thickness, as illustrated in Fig. 9. Representative EBIC line scans in a dislocated carbon-rich CZ sample and in EFG material when viewed in cross section are given in Figs. 10, 11, and 12. This technique of studying the sample cross section reveals for the first time the nature of L_n inhomogeneities in the bulk of the as-grown EFG sheet. Contrast of the L_n values measured in the two orientations shown in Fig. 9 often reflected the inhomogeneity, as surface values as high as 60-70 μm were obtained in some samples, while those in the cross section were much lower, perhaps 20-30 μm.

2. Annealing Studies

The four-point bending method produces a convenient range of dislocation densities in each wafer, with dislocation-free regions often remaining at the unstressed ends of the wafer. After the highest temperature anneals ($\geq$ 1200°C) even these dislocation-free regions were degraded by the thermal treatment alone, and the dislocation electrical activity was studied superimposed on this background. FZ silicon of non-detectable carbon and oxygen levels was compared to CZ silicon of about 1 x 10^{18}/cm^3 interstitial oxygen and varying carbon levels to examine the impact of these impurities on the diffusion length degradation and on the dislocation recombination changes after additional post-stressing anneals at 525°C and at 850°C for one hour. The effect of the thermal degradation also was studied separately by annealing samples in a double-walled quartz tube furnace, as compared to the stressed material which was produced in a regular crystal growth furnace.

Typical results for FZ silicon stressed at 1370°C (e.g., as in Fig. 5) that illustrate the trends observed in diffusion length with dislocation density and with annealing are given in Figs. 13 and 14. The diffusion length changed very little with dislocation density in samples heat treated and stressed above 1200°C; compare Fig. 13(b) to 14(a). This suggests that point defects dominate the recombination
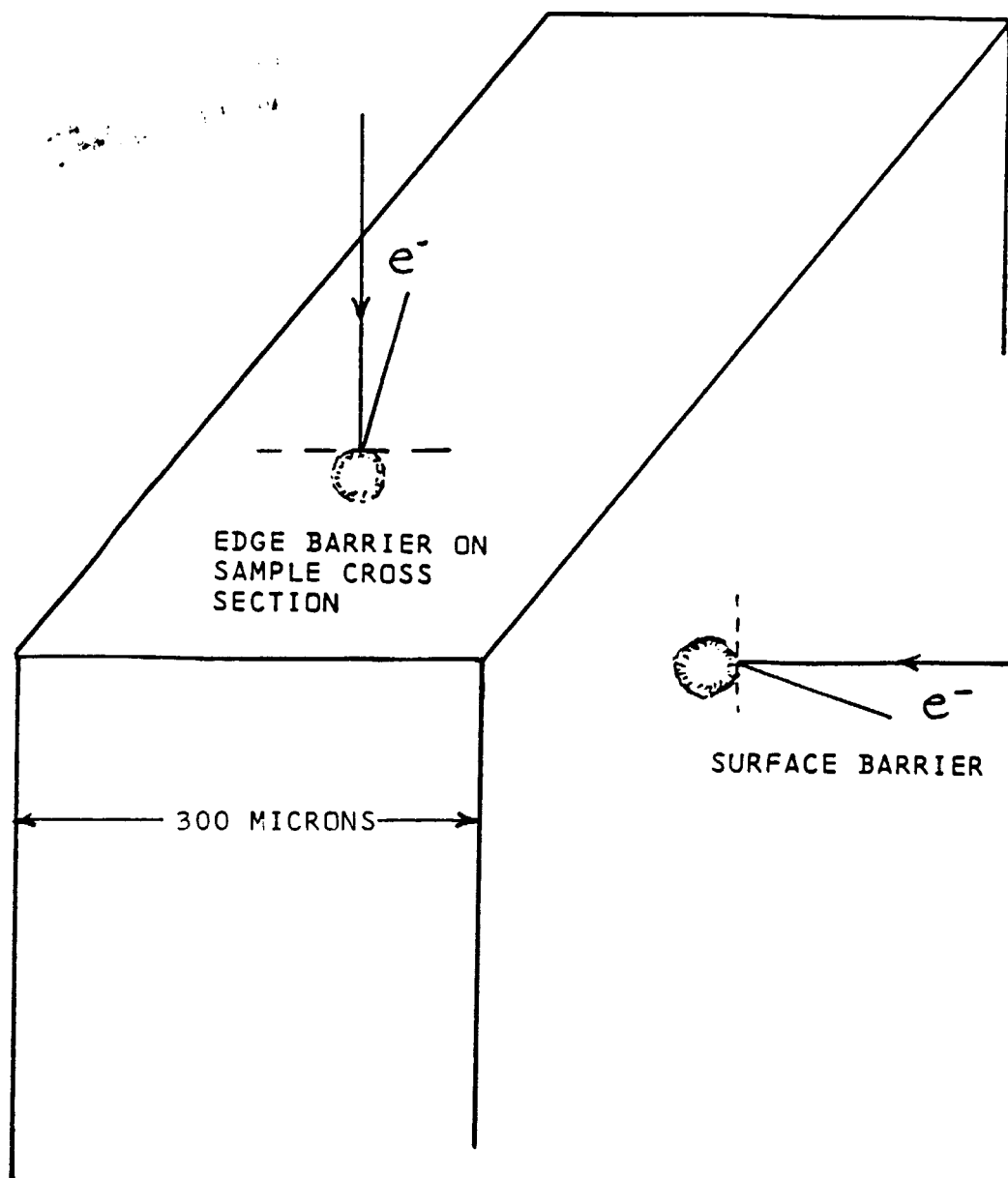
Fig. 9. Schematic illustrating EBIC technique application on sample cross section.
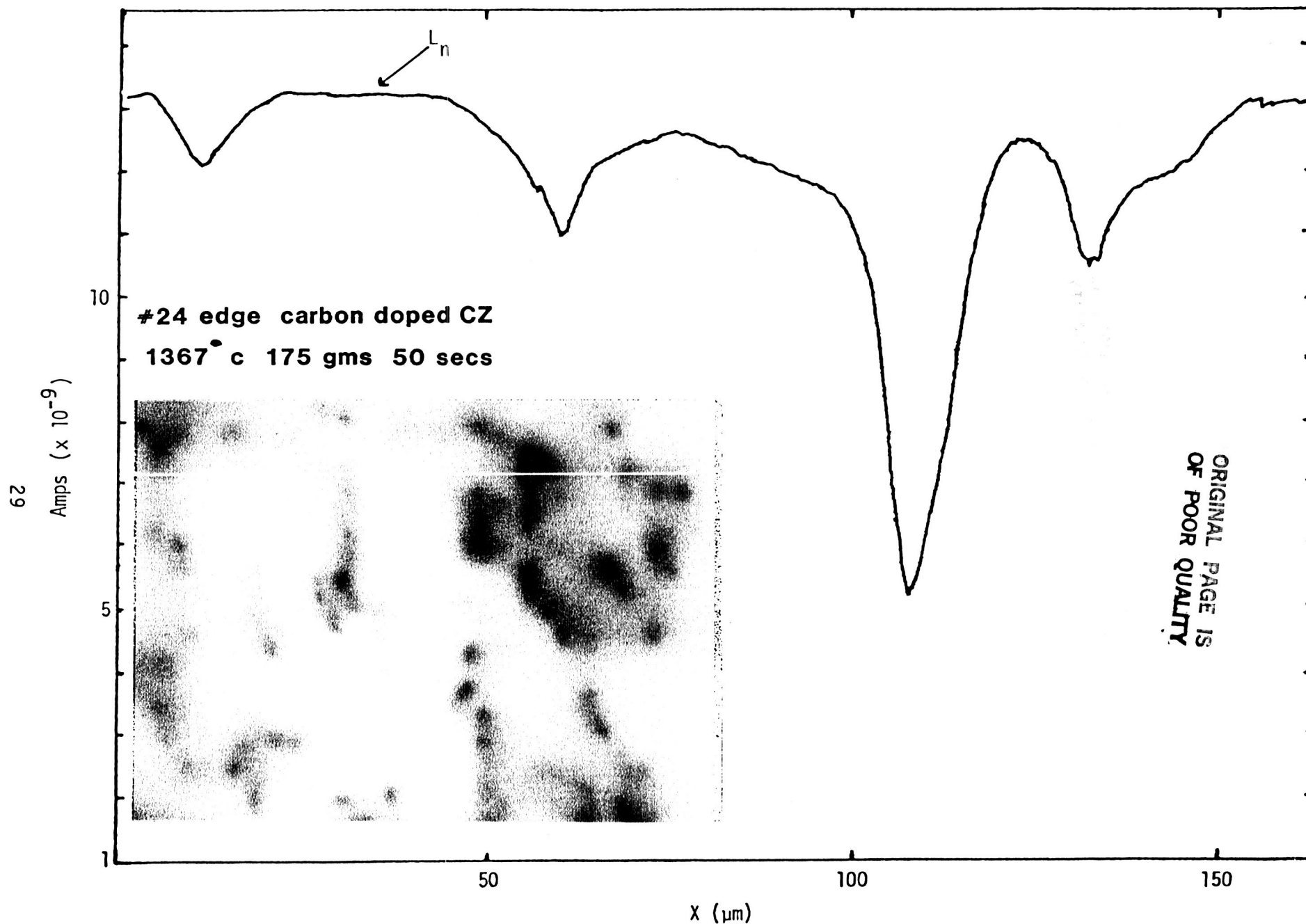
Fig. 10. High magnification (500X) low temperature EBIC line scan
of stressed carbon-doped CZ.

Distance across sample thickness (arb. units)
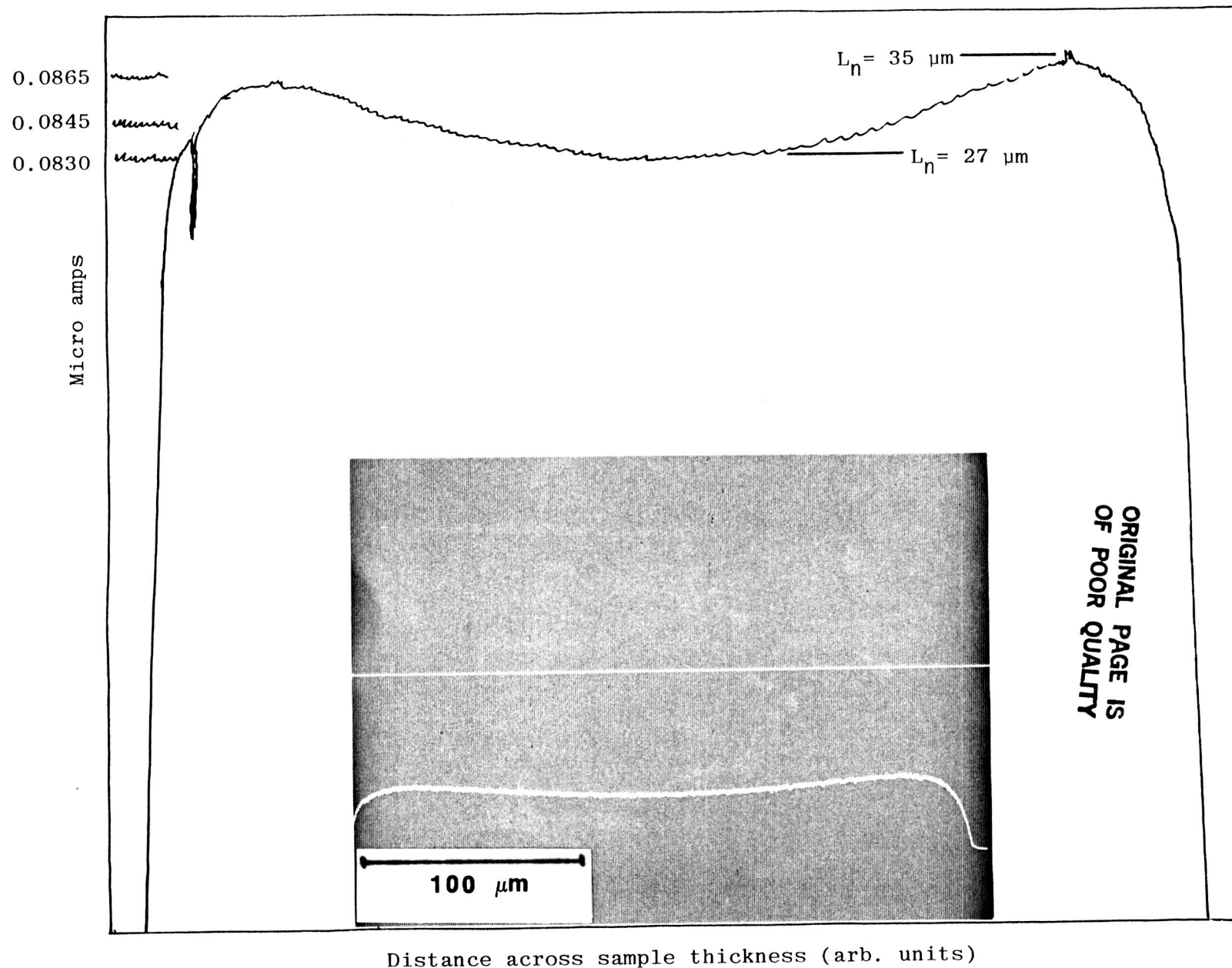
Fig. 11. High magnification (300X) room temperature EBIC line scan of EFG ribbon 17-S-20 in cross section for dislocation-free region.
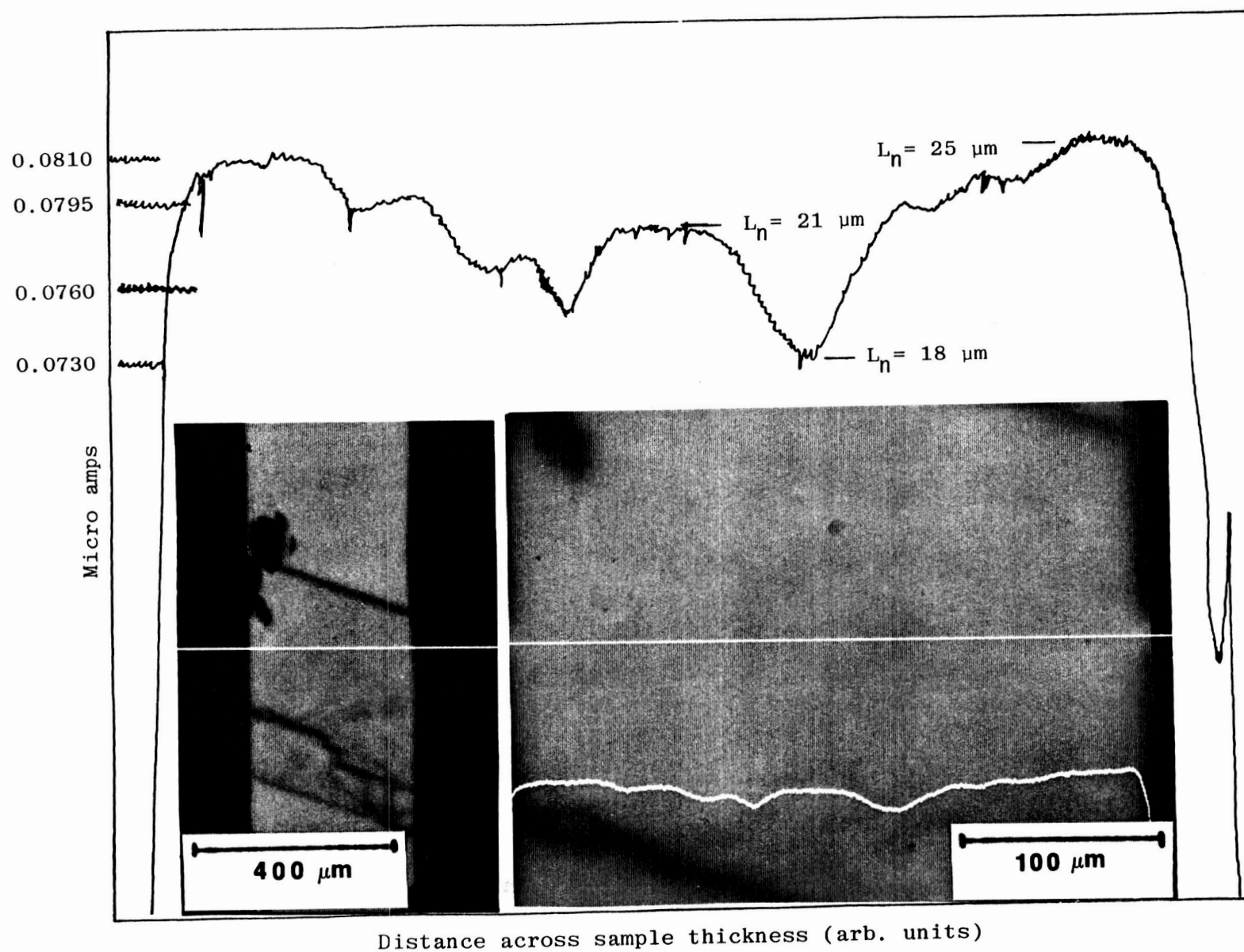
Fig. 12. High magnification (300X) room temperature EBIC line scan of EFG ribbon 17-S-20 in cross section for region with dislocations.

31
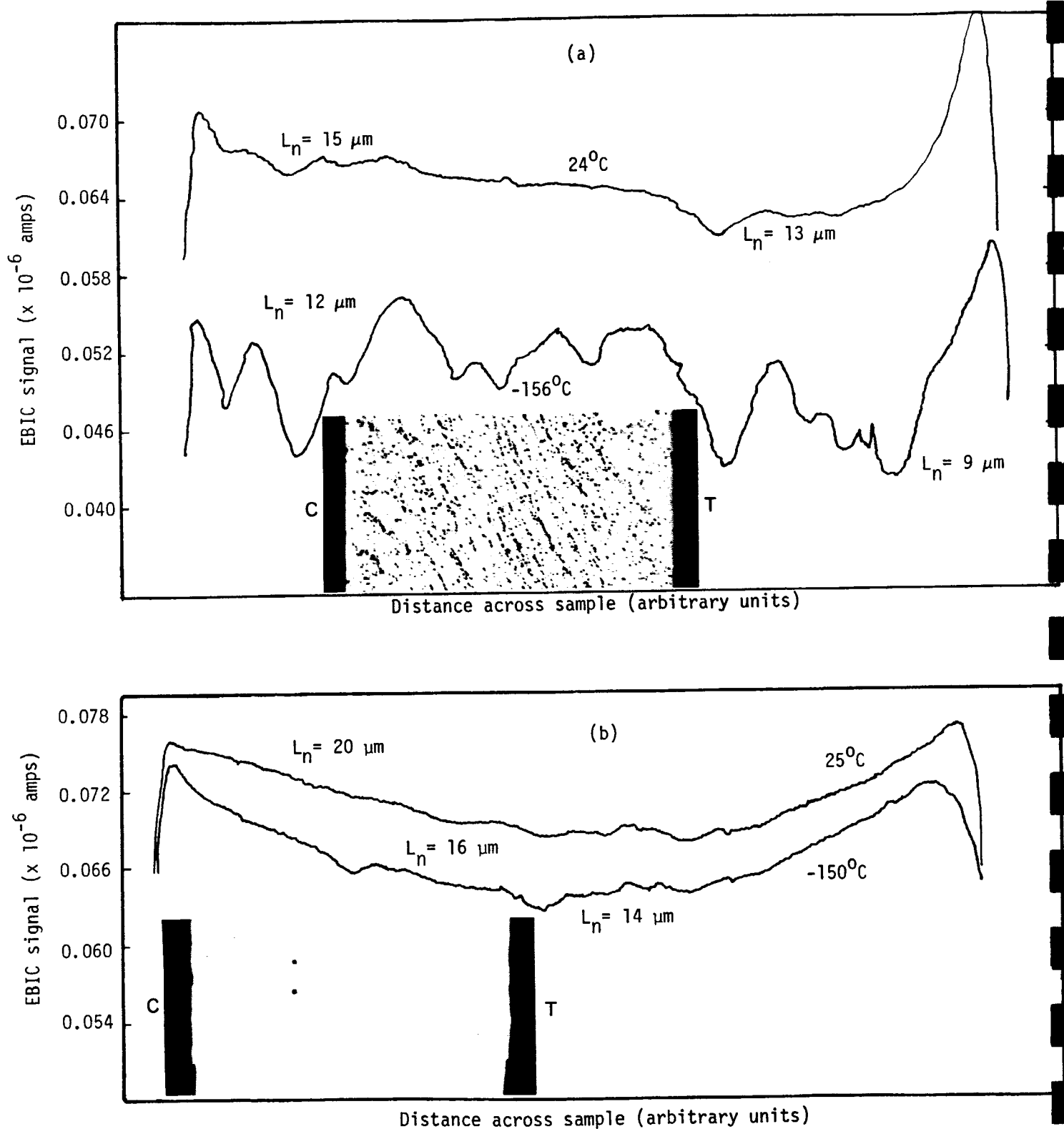
Fig. 13. EBIC line scans and photomicrographs of stressed FZ silicon:
(a) center sample #15C with $N_D \sim 1 \times 10^6/cm^2$; (b) end sample
#15E with $N_D \sim 1 \times 10^4/cm^2$. Tension surface is at right;
compression surface is at left.
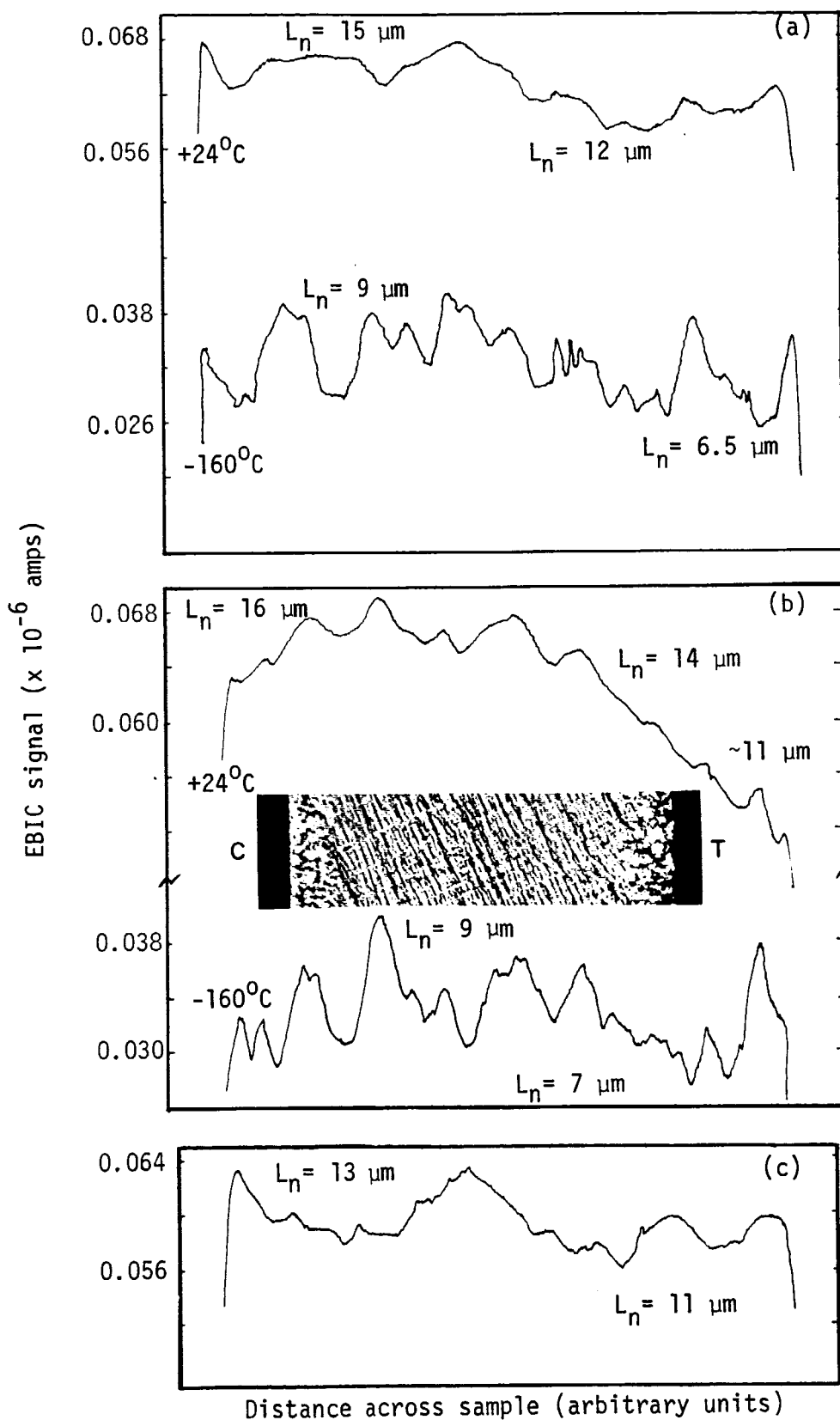
Fig. 14. EBIC line scans for stressed FZ silicon sample #17C in central high dislocation density ($\sim$1 x 10^7/cm^2) region: (a) after four-point bending at 1370°C; (b) after one-hour anneal at 575°C; (c) after one-hour anneal at 850°C.

after this treatment to pin the diffusion length at these low values, and dislocations have only a second order effect in limiting the diffusion length. Similar results were obtained in the CZ silicon wafers of vastly different oxygen and carbon concentrations, indicating that these impurities also have little impact on the diffusion length. The same relationships are observed at low temperatures. Figures 14(b) and (c) show that there is little change in the diffusion length after the one-hour anneals at 575°C and 850°C.

In general, some increases were observed after the 575°C anneal, but not the 850°C anneal. The CZ silicon tended to be more inhomogeneous in dislocation density and also not as reproducible in anneal response, as some larger increases (e.g., 20 to 40 μm) were observed in several samples after the one-hour anneal at 575°C for the less heavily dislocated regions.

The anneal experiments were repeated in a double-walled quartz tube furnace under vacuum, and similar low (~10 μm) diffusion lengths were found after a one-hour anneal at 1200°C. It was concluded that no specific impurity except possibly Fe was responsible for the diffusion length degradation, but that it likely arises mainly because of dissociation of bulk microdefects. The dislocated samples show that there are no strong gettering processes taking place in subsequent anneals which can restore the diffusion length to the as-grown values of the order of 150 μm. Again, the presence of oxygen and carbon as well as of dislocations does not have a large influence on the recombination sites produced in these samples.

3. Diffusion Length-Dislocation Density Correlations

The dislocation electrical activity effect on degrading diffusion length in the stressed samples is superimposed on the bulk diffusion length degradation produced by the heat treatment accompanying the four-point bending. Data obtained for different times and temperatures of stress application are summarized in Fig. 15. The times indicated are those for which the sample is under stress, and not the heat-up or cool-down times which are typically one-half hour each.
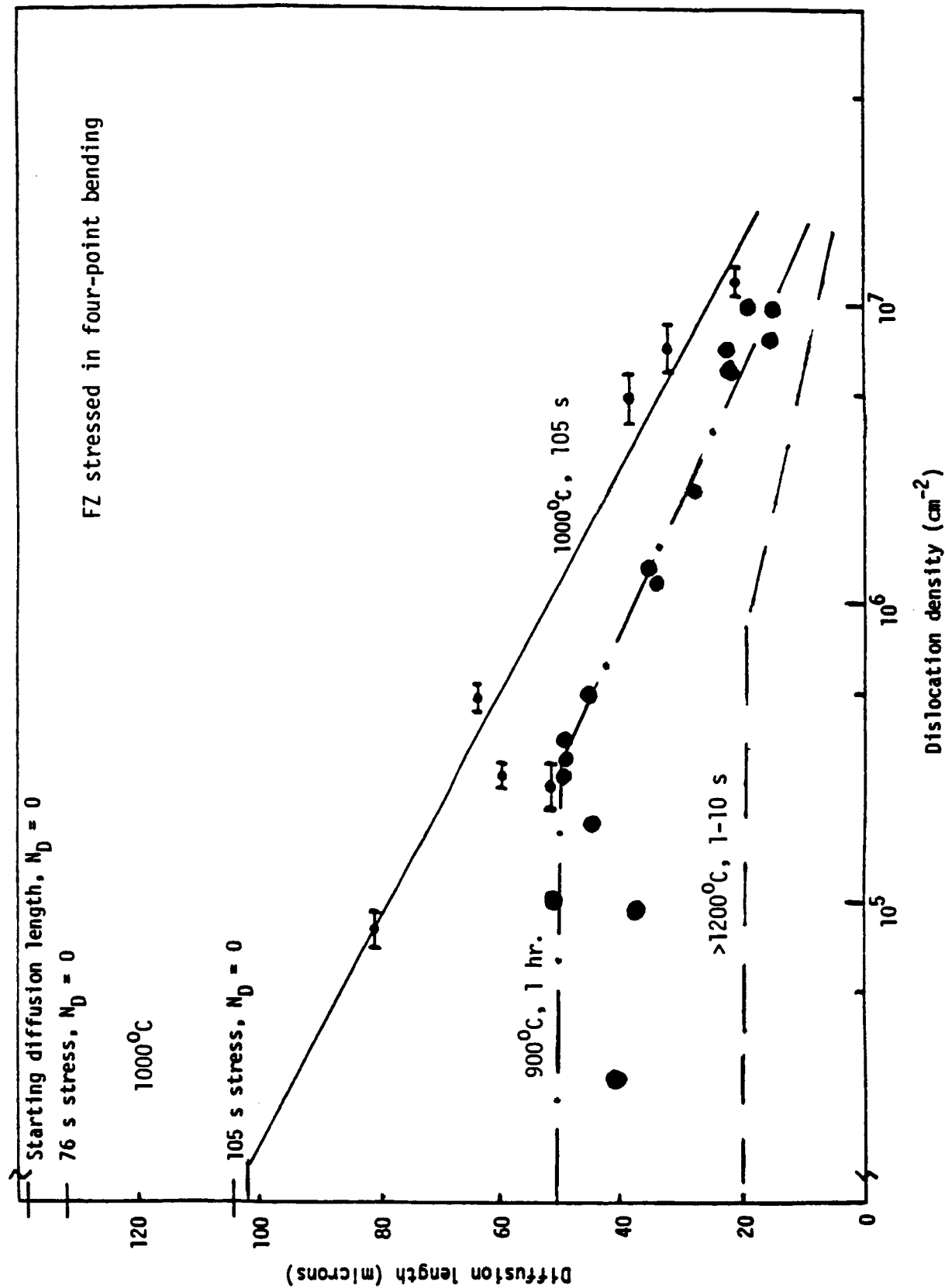
Fig. 15. Diffusion length dependence on heat treatment and dislocation density for FZ silicon.

The slope of the best fit line connecting the diffusion length at the dislocation density is somewhat different for the 900°C as compared to the 1000°C case, but both are close to a square root dependence.

The dependence of the diffusion length on dislocation density for the FZ silicon sample stressed at 1000°C is compared in Fig. 16 to relationships compiled for various other silicon materials and reported elsewhere [7]. All these data are distinguished by the fact that they fall above the line for which L_n is equal to the average spacing between dislocations, represented by the solid line $L_n = N_d^{-1/2}$ in Fig. 16. This is interpreted as signifying that the density of recombination sites associated with the dislocations is variable from case to case and that all sites are not electrically active.

The interrelation between the dislocation and point defect limitations on bulk lifetime is also evident from Fig. 16. At a given dislocation density, $1 \times 10^6/cm^2$, for example, there is no unique value for L_n. The latter ranges from low values of 20–30 μm for several types of high speed–grown silicon sheet, to above 150 μm in the best quality silicon. The latter generally has a bulk diffusion length of close to 1 mm in dislocation–free regions (L_n^o), as compared to 150–200 μm in the case of the highest values for sheet reported on small areas in CAST silicon ribbon.

The dislocation–free regions in the FZ stressed for 105 seconds at 1000°C had $L_n^o \simeq 100$ μm, in comparison. The slopes of the L_n vs. N_d curves and the dislocation density at which appreciable deviations from L_n^o are produced by the dislocations are a function of L_n^o. From Fig. 15 for the stressed FZ silicon, the thresholds for dislocation recombination are seen to vary from about $1 \times 10^4/cm^2$ when $L_n^o \simeq 100$ μm to about $1 \times 10^6/cm^2$ for $L_n^o \simeq 20$ μm.

None of the available data for other silicon as–grown material is complete enough to accurately delineate the L_n vs. N_d relationships in the region of interest here of dislocation densities between $1 \times 10^4/cm^2$ to $1 \times 10^7/cm^2$, and so they cannot be directly compared to the stressed FZ silicon. Investigators have taken lifetime τ to be
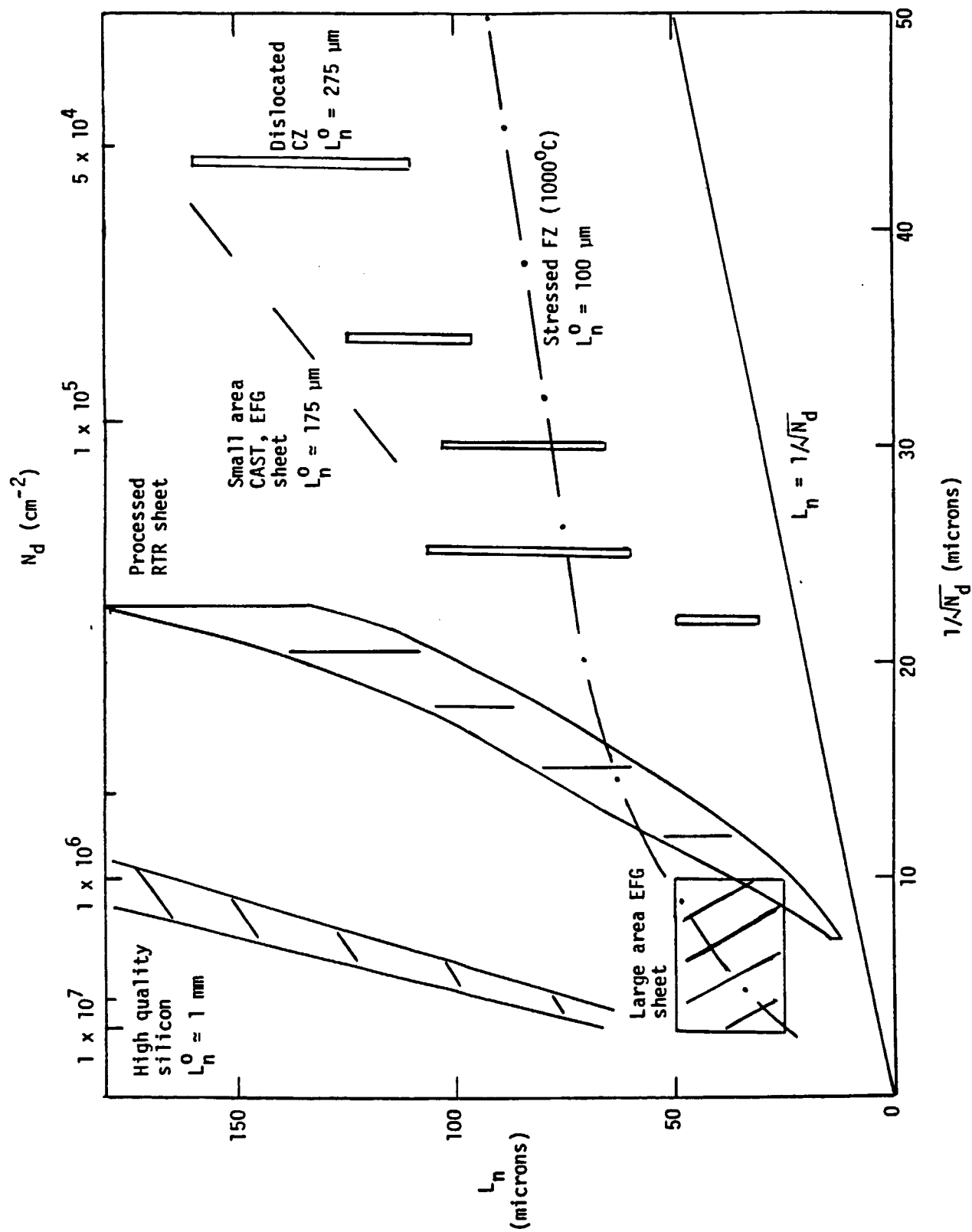
Fig. 16. Diffusion length dependence on dislocation density for several silicon materials.

inversely proportional to N_d in spite of the fact that the data is not accurate enough to warrant this assumption over large ranges of N_d in just about all cases. This gives $L_n \sim N_d^{-1/2}$. Our data for the stressed FZ silicon can be fit by $L_n = CN_d^{-1/4}$, implying $\tau \sim N_d^{-1/2}$.

Thus, there is the suggestion that the electrical activity of the creep-related dislocations produced by stress may differ fundamentally from that observed for grown-in dislocations, as represented by the more linear slopes of the other data in Fig. 16 for as-grown material. A possible explanation for this difference is that the creep-related dislocation electrical activity effects leading to bulk diffusion degradation also include contributions from dislocation "debris", i.e., point defect agglomerates, and are proportional to the total area swept out by the dislocations during the creep process.

Electron Paramagnetic Resonance (EPR) signals in dislocated silicon have been attributed to such debris [8], and it may be the factor that contributes to electrical activity outside of the dislocation core region itself, yet is directly related to the dislocation presence.

4. Low Resistivity Material

EBIC measurements of dislocation electrical activity were carried out at high magnification on low resistivity material. As discussed in Section C below, it is observed that dislocation etch pits increased significantly in size as the dopant concentration is increased. This is the case for both boron and gallium dopants. EFG material with normal 5 Ω-cm resistivities was therefore compared to 0.2 Ω-cm resistivity material up to magnifications of 10,000X on the basis of the profiles for recombination contrast around dislocations.

Typical results are shown in Fig. 17. The line scans across the single dislocations indicate that in all cases the core recombination region is broadened significantly for the low resistivity material, corresponding to the larger etch pit size. The increases in the region of high recombination as well as in the etch pit size could thus be related to dopant accumulation around the dislocation core. This data cannot distinguish between the two possible causes for these effects:

EBIC Signal

Scan distance x

1.0 μm

——— 0.2Ω-cm Gallium

········ 5.0Ω-cm Boron
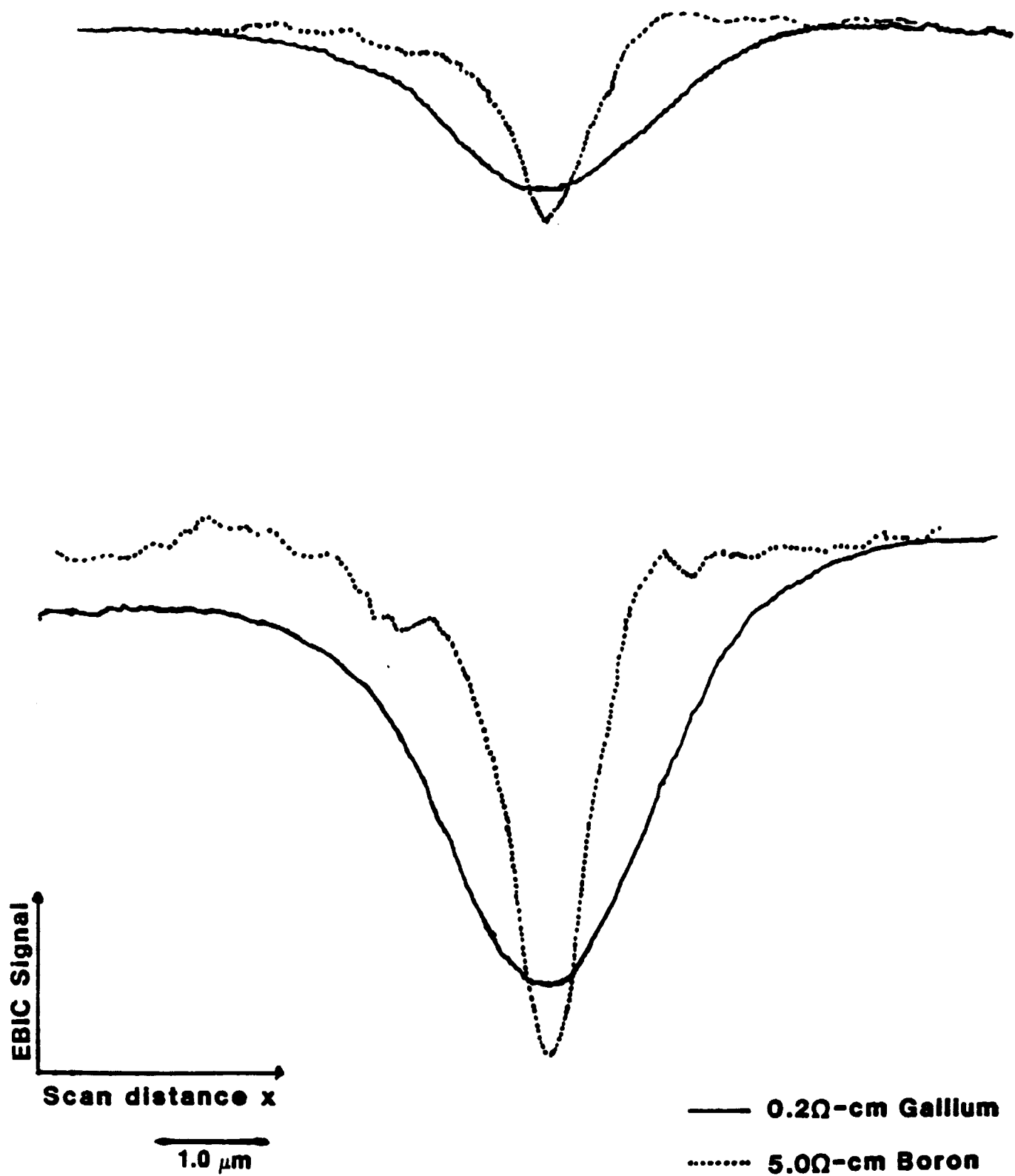
Fig. 17. EBIC line scans of dislocations in high
and low resistivity EFG Si ribbon.

either accumulation of dopant atoms themselves around the dislocation, or an increase in the dislocation strain field produced by dopant atoms, which then would perhaps attract more metallic impurities.

C. Low Resistivity Sheet Quality Studies
(M.C. Cretella, B.R. Bathey, and N.W. Marr)

This subtask was undertaken with the purpose of studying causes of degradation of the efficiency of non-single crystal silicon which occur with increasing base dopant level. This degradation is more severe in the more highly defected silicon under consideration for terrestrial solar cell manufacture than in FZ silicon. In the latter, maximum efficiencies are typically realized in the range 0.3-0.5 Ω-cm, below which Auger recombination starts to be a major factor in reducing performance. However, for a material such as Silso or EFG silicon, significant degradation below optimum performance levels achieved in the resistivity range 2-5 Ω-cm sets in at 1 Ω-cm. The degradation at higher resistivities is more severe in EFG material with a deficiency in oxygen, and this difference can be essentially eliminated above 2 Ω-cm with use of a silica crucible or by introduction of CO_2 in the growth ambient. Although oxygen leads to improvements in efficiency even at lower resistivities, it is not sufficient to raise efficiencies above the 5% level (no AR coating). The lower resistivity cells suffer both short circuit current and open circuit voltage degradation. Similar results have been reported for cast polycrystalline silicon, but the boron-defect-impurity interactions that may be responsible for degrading cell performance are not known.

The work done on the study of low resistivity EFG material on this program examined growth variable, phosphorus, boron and gallium dopant, and other impurity influence on the density of four types of defects commonly observed in as-grown material; dislocations, distinguished by Sirtl etching by their regular geometric shape and relatively deep pit, a small shallow pit quite distinct from that of the dislocation, some-times referred to as a saucer pit, and wing and line defects, which may have extensions of the order of 10 μm in cross-sectional etching.

40

The effects of dopants on defect density were first examined in 5 cm wide ribbon grown in the EFG test system described in Section IIA2b above. No identifiable variation of dislocation or other etch features were observed in this material, although material inhomogeneity made it difficult to obtain quantitative results. A very detailed study was made on boron-doped material grown at 2 cm/min in an induction heated furnace. The effects of oxygen addition during growth through use of a silica instead of a graphite crucible, and of adding Fe and Mo were also investigated. The results are summarized in Table II. The most significant findings were that the density of dislocation etch pits counted in the cross sections of ribbon samples decreases as a function of increasing impurity concentration for both the oxygen-lean case (graphite crucible) and the oxygen-enriched case (SiO_2 crucible); at the same time, however, the area of the etch pit developed with the standard Sirtl etchant -- for 30 seconds at room temperature -- increases with increasing dopant concentration.

It is clear from these data that the "line" defects occur significantly in only one sample set which is the 5 Ω-cm oxygen-lean material. Similarly, the "shallow saucer pits" occur in greater density over the whole range of impurity concentrations in the oxygen-lean material. These pits may be related to point defect clusters which are ascribed to the shallow pits observed in the swirl patterns in single crystal silicon.

The "wing" defects are generally associated with dislocation etch pits but at a lower density by an order of magnitude. The "wing" defect density does not appear to show any consistent correlation with the impurity levels in either the oxygen-lean or the oxygen-rich material.

One of the more surprising results obtained from the detailed analysis of defect densities with changes in total impurity added to the melt during growth is that for the cases of deliberate addition of Fe and Mo impurities (see Table II also). These large increases in added impurity do not produce significant changes in defect densities in many of the cases examined. Several exceptions are the general decreases in densities of dislocations and "wing" defects for the

41

Table II. Defect and Materials Property Characterization as a Function of Resistivity in Boron-Doped EFG Material.

Crucible Material	Measured Resistivity (Ω-cm)	Added Impurity (10^16 at/cc)	Impurity Element(s)	Avg. Area of Pit (10^-8 cm²)	Dislocation Etch Pits (#/cm²)	"Wing"(a) Defects (#/cm²)	"Line"(a) Defects (#/cm²)	Shallow Saucer Pits (#/cm²)	IR Spectrophotometer [O]_i (10^17 at/cc)	IR Spectrophotometer [C]_s (10^18 at/cc)	IR Spectrophotometer SiC Peak Area (Surface Film)	Combustion Analysis O_Total (10^18 at/cc)	Combustion Analysis [C]_Total (10^19 at/cc)	L_n (µm)
Graphite	5.0	0.28	B	2.3	6.0E6	2.3E4	5.6E4	3.5E7	<.2	1.7	.6	.2–.3	2.5	45
	1.24	1.8	B	2.7	4.3E6	5.9E4	*	4.9E7	<.2	1.3	.3	N.D.–.2	3.0	48
	0.17	20.0	B	3.5	2.9E6	4.2E4	*	2.7E7	<.2	1.7	.4	.2–.3	5.0(b)	22
	0.17	200.0	B,Fe,Mo	3.1	3.3E6	5.3E4	*	6.7E7	no transmission	no transmission	no transmission	N.D.	4.8	
SiO₂	4.6	0.25	B	1.4	17.E6	7.E4	1E4	1.0E7	2.4	1.7	1.6	.9	3.3	38
	1.04	1.8	B	1.7	8.9E6	14.E4	*	1.8E7	1.2	1.0	1.6	.9	4.0	40
	.16	21.0	B	3.3	4.6E6	15.E4	2E4	**	.8	N.A.	N.A.	1.1	4.2	27
	.17	110.0	B,Fe	4.0	3.1E6	2.E4	4E4	0.84E7	.9	N.A.	N.A.	1.7	4.3	15
	.17	600.0	B,Fe,Mo	3.6	1.2E6	.5E4	8E4	0.82E7	no transmission	no transmission	no transmission	.7	3.7	16

(a) These defects are not uniform over cross section. Values represent average densities over full thickness for locations where the defect is found. Less than 20% of cross section shows these defects.

(b) High SiC particle density.

* No defects observed.

** Not counted.

N.A. Not available.

N.D. Not determined.

quartz crucible-grown (oxygen-rich) ribbon, where general trends established with increasing boron levels are continued. In contrast, essentially no changes in the densities of these two defects occur for the oxygen-lean ribbon. Of particular interest are the results for the shallow saucer pits. These comprise the dominant etch feature, and it is surprising that their densities are not altered in proportion to the factor of ten changes in total added impurity. One explanation is that the iron and molybdenum, and perhaps even the boron, do not perturb the point defect equilibria and/or nucleation processes responsible for these microdefects because they are still governed by carbon or carbon/oxygen effects.

Gallium-doped material has been grown over a similar range of resistivity and impurity conditions as the boron-doped material. Although a higher diffusion length (30-50%) was measured on the Ga-doped blanks, the solar cells by our standard process did not show any better performance than B-doped material. Thus, standard processing techniques -- developed for B-doped materials -- do not preserve the lifetime advantage associated with the Ga-doping.

Analysis of the defect concentrations in the gallium-doped material indicated no consistent trends with impurity concentration. In general, at high resistivities, > 1 Ω-cm, the dislocation etch pit density is about a factor of two lower than that found for B-doped material while at low resistivities, ~0.2-0.6 Ω-cm, the etch pit density is nearly a factor of three greater for the Ga-doped case. "Line" and "wing" defects occur more homogeneously and over the whole range of doping concentrations. "Shallow saucer pits" appear to be uniformly greater by about an order of magnitude for the Ga-doped case.

D. <u>Residual Stress Measurements</u> (A. Andonian, S. Danyluk at U. of Illinois (Chicago), and L. Bucciarelli, MIT)

After it was demonstrated that laser interferometry may be used to evaluate residual stress distributions on a macroscopic scale in CZ silicon wafers, a project was started with the University of Illinois at Chicago to develop appropriate modifications of the technique so that it could be applied in the case of rectangular EFG

43

blanks. This offered several new challenges in that EFG material has more irregular dimensions, that include thickness nonuniformity and surface striations which produce deviations from flatness significant enough to complicate the fringe patterns generated.

A shadow Moiré technique was found to be most suitable for measurement of residual stress in the EFG material. As part of this effort, an approach to relate redistributed stress in finite size blanks to the original stress distribution in a semi-infinite as-grown finite width sheet was developed at MIT. A paper attached as Appendix II gives a summary of the main results of this project. Other details may be found in the reports of subcontract No. 956053 of the Advanced Materials Research Task of the FSA Project of work carried out at the University of Illinois.

III. CONCLUDING REMARKS

Efforts were not successful to find an operating "window" for EFG silicon sheet growth that would allow growth speeds to exceed 2-3 cm/min without generating thermoelastic stress levels that produce unacceptable deviations from flatness, high residual stress and higher defect densities. However, considerable progress was made in the understanding of stress generating mechanisms. This will help in directing future research and development work toward construction of lower stress EFG systems, provided that growth speeds are not pushed above the 2 to 3 cm/min range.

Much of the difficulty encountered in the search for lower stress high speed EFG growth configurations (i.e., those allowing growth above 3 cm/min) was a general lack of flexibility to make large modifications of the post-growth cooling environment, such as dictated by the stress analysis, without a concurrent loss in growth stability. This inflexibility essentially prevented verification of a number of aspects of the stress analysis because only a very narrow range of growth conditions was achievable in any one growth system.

The stress and temperature modeling clearly demonstrated that large second derivatives in the temperature profile, hence high initial stress levels, are closely interrelated with high interface temperature gradients, and that it is the fundamental heat transfer conditions for silicon that do not allow for extraction of the latent heat of fusion at rates great enough to maintain growth speeds of 3 cm/min and above without also producing the high temperature profile curvature. Then it becomes only a question of how intense is the creep that takes place in a very narrow region within about 5 mm of the interface: This creep prevents catastrophic stress levels from being reached very quickly in the first few cm of growth, so that

45

buckling cannot occur. This is the nature of the "creep limitation" to silicon sheet growth which is likely to be generic to all modes of "vertical" pulling, i.e., growth where the liquid-solid interface is perpendicular to the pulling direction to within a few degrees.

On the other hand, the stress analysis has shown that considerable potential exists to reduce stress in EFG systems, provided growth speed is maintained below values where the near-interface region creep limitations are felt. This is estimated to be in the range of 2 to 3 cm/min, depending on sheet width and thickness. The potential to produce large stress reductions with cooling of the edge of the sheet with respect to the centerline is demonstrated to exist. The quantitative details of the stress reductions depend on the creep relaxation, which is not known for the temperature region below 1200°C. Initial measurements of stress relaxation in silicon of these lower temperatures have been obtained and need to be formulated into a creep law.

The EBIC technique was successfully applied to obtain a quantitative evaluation of the effect of dislocation electrical activity limitation on minority carrier diffusion length. Correlations between diffusion length and dislocation density were obtained for FZ silicon stressed at several temperatures above 800°C. It was found that the relationship $L_n \sim N_d^{-1/4}$ best described the results. This dependence is different from the results given for as-grown dislocation effects, where $L_n \sim N_d^{-1/2}$. These results suggest that the electrical activity of creep-related dislocations includes effects from dislocation "debris" that is created in the creep process, and thus their electrical activity also depends on the intensity of the creep, namely the area swept out by the dislocation.

Low resistivity EFG material was studied by examining defect density and dislocation electrical activity dependence on dopant concentration for boron and gallium. The main findings were that the dislocation density decreased with increasing dopant concentration but that etch pit size increased. The latter effect was corroborated with EBIC characterization, where the region of high recombination around

46

the dislocation was observed also to increase with increasing dopant concentrations. Although as-grown diffusion lengths for gallium-doped EFG material were generally higher than that for boron dopant, increases in solar cell performance were not obtained. Some differences in defect densities between gallium and boron dopant were observed.

A shadow Moiré technique of laser interferometry to measure residual stress in EFG material was developed in collaboration with the University of Illinois (Chicago) and used to study stress distributions in 10 cm x 5 cm samples.

References

1. J.P. Kalejs et al., July–September 1982 Quarterly Progress Report, DOE/JPL 956312/01.

2. J.P. Kalejs et al., October–December 1984 Quarterly Progress Report, DOE/JPL 956312/06.

3. J.P. Kalejs et al., January–March 1985 Quarterly Progress Report, DOE/JPL 956312/11.

4. J.P. Kalejs et al., April–June 1983 Quarterly Progress Report, DOE/JPL 956312/04.

5. J.P. Kalejs et al., January–March 1984 Quarterly Progress Report, DOE/JPL 956312/07.

6. J.P. Kalejs et al., July–September 1984 Quarterly Progress Report, DOE/JPL 956312/09.

7. U. Gösele, J.P. Kalejs and L.A. Ladd, Abstract No. 308, ECS Meeting, Boston, May 4–9, 1986.

8. P. Omling et al., Phys. Rev. B, 32 (1985), 1571.

9. J.P. Kalejs et al., October–December 1985 Quarterly Progress Report, DOE/JPL 956312/14.

APPENDIX I

Bibliography of Publications Generated
During the Program

1. H.M. Ettouney and R.A. Brown, "Mathematical Modeling of High Speed Ribbon Systems: A Case Study of Edge-Defined Film-Fed Growth", in: Proc. Flat-Plate Solar Array Project Research Forum on High Speed Growth and Characterization of Crystals for Solar Cells, ed. K.A. Dumas, DOE/JPL 1012-95 (April 1984), (Jet Propulsion Laboratory, Pasadena, CA, 1984), p. 311.

2. J.W. Hutchinson and J.C. Lambropoulos, "The Effect of Creep on the Residual Stresses Generated During Silicon Sheet Growth", ibid., p. 351.

3. J.P. Kalejs and R.O. Bell, "Experimental Aspects of the Study of Stress Generating Mechanisms in Silicon Sheet Growth", ibid., p. 367.

4. J.C. Lambropoulos, J.W. Hutchinson, R.O. Bell, B. Chalmers and J.P. Kalejs, "Plastic Deformation Influence on Stress Generated During Silicon Sheet Growth at High Speeds", J. Crystal Growth, 65 (1983), 324.

5. H.M. Ettouney, J.P. Kalejs and R.A. Brown, "Comparison of Finite Element Calculations and Experimental Measurements in Edge-Defined Film-Fed Growth of Silicon Sheets", J. Crystal Growth, 70 (1984), 306.

6. P.A. Mataga, J.W. Hutchinson, B. Chalmers, R.O. Bell and J.P. Kalejs, "Effects of Transverse Temperature Field Nonuniformity on Stress in Silicon Sheet Growth", to be published in J. Crystal Growth as part of special volume "Proceedings of the First International Symposium on Shaped Crystal Growth: Stepanov, EFG and Other Techniques".

7. Y. Kwon, S. Danyluk, L. Bucciarelli and J.P. Kalejs, "Residual Stress Measurement in Silicon Sheet by Shadow Moiré Interferometry", to be published, ibid.

APPENDIX II

Paper titled "Residual Stress Measurement in Silicon Sheet by Shadow Moiré Interferometry" by Y. Kwon, S. Danyluk, L. Bucciarelli, and J.P. Kalejs.

This paper was presented at the First International Symposium on Shaped Crystal Growth held in Budapest, Hungary, July 22-25, 1986, and published in a Proceedings Volume of the Journal of Crystal Growth.

Residual Stress Measurement in
Silicon Sheet by Shadow Moiré Interferometry

Y. Kwon and S. Danyluk
Department of Civil Engineering, Mechanics and Metallurgy
University of Illinois at Chicago
Chicago, Illinois 60680, U.S.A.

L. Bucciarelli
School of Engineering
Massachusetts Institute of Technology
Cambridge, Massachusetts 02139, U.S.A.

and

J.P. Kalejs
Mobil Solar Energy Corporation
16 Hickory Drive
Waltham, Massachusetts 02254, U.S.A.

A shadow Moiré interferometry technique has been developed to measure residual strain in thin silicon sheet. The curvature of a segment of sheet undergoing four-point bending is analyzed to include the applied bending moments, the in-plane residual stresses, and the "end effect" of the sheet since it is of finite length. The technique is applied to obtain residual stress distributions for silicon sheet grown by the Edge-defined Film-fed Growth technique.

1. Introduction

The Edge-defined Film-fed Growth (EFG) technique is currently being used to produce silicon sheet for photovoltaic applications. Growth conditions such as the temperature distribution in the sheet place constraints on the sheet growth velocity, its thickness, and width because nonuniform temperature fields produce in-plane and out-of-plane stresses in the sheet. Thermoelastic stress, if sufficiently large, leads to buckling during growth [1] and to the generation of dislocations and permanent plastic deformation [2].

Conventional thermoelasticity theory has been used to predict static stress distributions in long, thin strips of finite width sheet subjected to a nonuniform temperature distribution, in order to simulate stress produced in silicon sheet during growth, with useful results [3]. This analysis has recently been extended to include the effects of plasticity through incorporation of dislocation dynamics for low strain deviations from elasticity [4]. These models do not lead to correct predictions for residual stress of sheet grown with plastic deformation, which is often found to be operative [1]. A full steady-state treatment of thermoelastic effects in thin sheet growth with plastic deformation has been developed [2], which relates residual stress to the temperature distributions imposed on the sheet in growth and to creep behavior. The residual stress distributions obtained from all these analyses are those for a semi-infinite sheet, i.e., a long segment of finite width, one end of which is at the melting point of silicon and the other is at room temperature.

EFG silicon sheet of 5 cm width is often processed into solar cells by cutting it into 5 cm x 10 cm shorter segments, or blanks. This sectioning relieves and redistributes grown-in residual stress. Out-of-plane stress most often deforms the blanks by twisting. In-plane residual stresses promote slow crack growth or fast fracture by the propagation of microcracks that occur in the cut edges. The detection and measurement of the in-plane residual stresses in short sections of sheet is a means by which information on stresses present during growth can be obtained. However, care must be taken that the effects of stress redistribution in cutting are taken into account if measured stresses in the cut sections are to be compared to the predictions of the stress analysis for the growing sheet.

56

In this paper, we report on the application of a shadow Moire interferometry technique for the measurement of the in-plane residual stresses in short, thin and flat plates. The technique is non-destructive and can be applied to large areas of EFG silicon sheet when external deformation cannot be used to deduce the in-plane residual stress. In Section 2 we describe the analysis that is used to obtain redistributed strain and stress distributions in the finite segment of a cut blank of 5 cm wide sheet, and the experimental details of the measurement for EFG material. Results on the stress distributions measured in EFG silicon sheet are reported in Section 3. The technique limitations and relation of measured stresses to growth variables are examined in Section 4.

2. Description of the Technique

The technique measures strains in short segments of sheet and uses an analysis incorporating nonlinear elasticity theory to extract the residual stresses. The analysis used to obtain residual stress has been described previously [5], and is applied here to the case of a rectangular (5×10 cm^2) plate geometry typical of cut blanks of silicon sheet grown at a 5 cm width.

2.1. Analysis

We consider a thin, short, flat plate whose width is half its length, containing in-plane residual stresses represented by the stress component σ_{xx}, shown in Fig. 1. These stresses must decrease to zero at the ends if they are to be traction free. The plate, by necessity, must contain a "shear flow" that compensates for this decrease of the in-plane residual stresses. This is the stress component σ_{xy}. We take for the

stress calculation a shear flow that is linear along the length of the plate and apply a known bending moment to the plate. We can then calculate the plate deflection as a function of its geometry and flexural rigidity, the applied bending moment and residual stresses. We have carried out this analysis for the geometry shown in Fig. 2 [5] with governing equations for the curvature when the plate is in in-plane tension and compression (represented by P):

$$\frac{d^2w}{dx^2} = -\frac{M}{D} - \frac{P}{D} w + \frac{AP}{2D} (x_o^2 - Lx_o) \qquad \text{in-plane tension} \qquad (1)$$

$$\frac{d^2w}{dx^2} = -\frac{M}{D} + \frac{P}{D} w - \frac{AP}{2D} (x_o^2 - Lx_o) \qquad \text{in-plane compression} \qquad (2)$$

where M is the applied bending moment, D is the flexural rigidity ($D = Eh^3b/12(1 - \nu^2)$), E is Young's modulus, ν is Poisson's ratio, h is the thickness, b is the width, L is the length, and w is the measured deflection of the plate at x_o. The curvature is $d^2w/dx^2 = 2A$ (to be determined experimentally) if the defection is assumed to be polynomial ($w = Ax^2 + Bx + C$). E = 165 GPa and ν = 0.3 were used here for stress calculations.

A method has been developed to relate the residual stress distribution in a semi-infinite sheet of natural width of 5 cm, such as predicted by finite element analysis [2], to the redistributed stress in the 5×10 cm^2 blank to be measured which is cut from this sheet. The approach used is similar to that presented by Horvay [6]. Details of this analysis as applied to the geometry of interest here is given elsewhere [7]. The starting point of the analysis is an arbitrary stress

distribution $\sigma_{xx}(y)$ in a semi-infinite sheet of width b, an example of which is presented in Fig. 3. When a short segment of length L is cut out of the semi-infinite strip, the interior of this segment is still subjected to the initial distribution in the uncut segment. To account for the creation of the free ends in the finite length piece, a stress distribution equal and opposite to the initial residual stress distribution must be superimposed at each end. The solution to this stress boundary value problem, superimposed on the original residual stress state, gives the stress distribution in the cut, finite sheet segment.

The predicted redistributed stresses are given in Fig. 4 for a section of a cut blank of length to width ratio $L/b = 2$ for an initial stress distribution as shown in Fig. 3. An important result for the stress measurements is that the shear flow stress component σ_{xy} obtained does not depart markedly from the form taken previously for the calculation of the stress distribution from the strain [5]. σ_{xy} is identically zero on the blank centerline (Fig. 4a), and has appreciable non-zero values starting at a distance of about one blank half-width from the end for the blank interior ($y/b = 0.5$), as in Fig. 4b. As part of the stress redistribution at the blank end, the σ_{xx} decreases to zero while σ_{yy} increases to levels comparable to the maximum amplitude for σ_{xx} in the blank before cutting. The σ_{yy} distribution across the width at the blank end is shown to be quite complicated [7] and the shear flow in general will be a function of the initial σ_{xx} distribution and of L/b. When L/b is decreased to the order of unity and below, the end effects start to decrease the maximum stresses in the blank to significantly below those found in the uncut strip. The present technique measures σ_{xx} only.

2.2. Experimental Details

The experimental technique consists of bending a 5 x 10 cm EFG blank in a four-point bend apparatus, measuring the bending moment by a load cell and recording surface fringes produced through an optical grating illuminated by an He-Ne laser (Fig. 2). The grating has 8 lines per mm. A 2.2 kg load is applied for the data taken here. The surface image contains fringes caused by the interference of the grating and the shadow (shadow Moire technique). The density and spacing of the fringes form a topographic map of the sample. Their contrast is enhanced by applying a thin coating of paint to the as-grown EFG blank surface. A cubic spline technique is used to generate an analytic expression for the curvature at each point on the sample. This measured curvature is compared to the curvature that is expected when there are no in-plane residual stresses in the sheet (i.e., $d^2w/dx^2 = -M/D$). If the measured curvature is larger than this analytically derived curvature, then the in-plane residual stresses must be compressive and Eq. (2) is used to solve for P. If the converse is true, then Eq. (1) is used to obtain P.

3. Results

This technique has been applied to obtain stress in 5 cm wide EFG sheet grown at two different speeds. Figures 5 and 6 show interferograms and the in-plane residual stress distributions at several selected positions in a section of sheet 10 cm in length cut along the growth direction. The low stress sample grown at $V = 1$ cm/min shows that the residual stresses in the lower half are approximately 2 MPa while the high stress sample grown at $V = 2$ cm/min contains a maximum residual stress of approximately +5 MPa in the center and -8 MPa at the outer edge.

An example of an extended map of the residual stresses in a 2.5 cm x 2.5 cm section of a 5 cm x 10 cm blank adjacent to the centerline x = L/2 is shown in Fig. 7. This indicates a maximum tensile stress of ~8 MPa in the center and a compressive stress of ~8 MPa at the outer periphery of the blank.

4. Discussion

The measured stress distributions in the 5 x 10 cm^2 EFG blanks, represented by the data of Figs. 5-7, exhibit general features of those predicted by finite element analysis of steady-state EFG silicon sheet grown under conditions of intense creep [2], which are of the form shown in Fig. 3. However, they differ qualitatively from those predicted for conditions of mild creep or on the basis of the thermoelastic theory alone. These differences warrant a more detailed inspection of the experimental results, and of possible limitations of the stress measurement technique for the present application.

Inhomogeneities in EFG material dislocation distributions [8] indicate that uniform stress relaxation does not take place in growth. The extent of the nonuniformity is best illustrated by the detailed mapping in Fig. 7. The variations across the width (y) are expected on the basis of the stress analysis of steady-state semi-infinite sheet growth, but the variations along the growth direction (x) are outside of the scope of this analysis. The observed variation can be accounted for by nonuniform creep. If stress relief by intense creep at a given transverse (y) location in the growing sheet is accompanied by rapid redistribution of the stresses, the new distribution will lead to subsequent creep not predicted by the

61

steady-state analysis [2]. Such redistribution could be triggered by thermoelastic stress levels that exceed the upper yield stress and produce rapid dislocation multiplication, hence fast stress relief, in a localized area in which the matrix is very susceptible to these processes of stress relief. The redistribution of stresses accompanying this stress relief could then tend to shield nearby regions from undergoing similar intense creep relaxation until a sufficient additional section of the sheet is formed to again build up high stresses.

The data of Figs. 5 and 6 indicate that residual stress levels are greater at the higher growth speed. Generally, the post-grown cooling profile is adjusted so as to increase the interface-region temperature gradient in order to ensure that acceptable growth stability is maintained as speed is raised. The increases in residual stress observed are probably a consequence of associated increases in temperature field nonuniformities which lead to higher thermoelastic stress levels.

The quantitative predictions of stress measurement made on EFG sheet must be treated with some caution. A linear approximation for the shear flow is used in the stress calculations, since the form of σ_{xy} in Fig. 4 is not known a priori. The blanks are not of a regular geometry and also are not single crystal. Each of these factors introduces uncertainty in the absolute stress determinations. The problems created by irregularities in surface topology are evident in the interferograms of Figs. 5 and 6. The fringes would be regularly spaced for a flat surface, and the deviations shown there impact on accurate fringe spacing measurements, hence strain and stress determination. Non-flatness also precludes use of finer optical

gratings, which could increase the resolution below the level of 0.2 to 0.4 MPa estimated for the present measurements. The blank also often is nonuniform in thickness [1]. Since thickness enters to the third power in the calculation of D in Eqs. (1) and (2), very accurate local measurements of thickness are required in order to keep errors in the stress small. Finally, the technique does not take into account anisotropies in E and ν which are present in non-single crystal specimens such as the EFG material. These constants vary significantly as a function of crystal orientation in silicon [9], by as much as a factor of two in some cases. EFG material surface orientation is close to (110), however, and consists mainly of twinned regions that only deviate by 10-15° on average from <110>. Anisotropies in E and ν are not as severe around <110> as in other directions.

The distributions obtained for EFG silicon sheet in Figs. 5-7 are qualitatively similar to results reported for silicon ribbon grown by the Edge Stabilized Ribbon (ESR) technique, where the stress measurements were made using a method utilizing infrared birefringence [10].

Acknowledgements

63

References

1. J.P. Kalejs, B.H. Mackintosh and T. Surek, J. Crystal Growth, 50 (1980), 175.

2. J.C. Lambropoulos, J.W. Hutchinson, R.O. Bell, B. Chalmers and J.P. Kalejs, J. Crystal Growth, 65 (1983), 324.

3. R.G. Seidensticker and R.H. Hopkins, J. Crystal Growth, 50 (1980), 221.

4. O.W. Dillon, C.T. Tsai and R.J. DeAngelis, this Proceedings Volume.

5. A.T. Andonian and S. Danyluk, J. Mater. Sci., 20 (1985), 4459.

6. G. Horvay, J. Appl. Mech., 87 (1953), 87.

7. J.P. Kalejs et al., Quarterly Progress Report DOE/JPL 956312/13 (July 1, 1985-September 30, 1985), January 15, 1986.

8. C.V.H.N. Rao, M.C. Cretella, F.V. Wald and K.V. Ravi, J. Crystal Growth, 50 (1980), 311.

9. J.J. Wortman and R.A. Evans, J. Appl. Phys., 36 (1965), 153.

10. E. Sachs and D. Ely, 17th IEEE Photovoltaic Specialists Conference Record (IEEE: New York; 1984), p. 1418.

Figure Captions

Fig. 1. Idealized residual stress representation in a thin plate containing a heterogeneous in-plane stress.

Fig. 2. Schematic of the experimental arrangement used in the shadow Moiré interferometric technique of residual stress measurement.

Fig. 3. Residual stress distribution in semi-infinite ribbon used in calculation of end effects. σ_{yy} and σ_{xy} are identically zero.

Fig. 4. Residual stress component variations in the growth direction (a) along the blank centerline ($y = 0$) and (b) half-way to the blank edge ($y/b = 0.5$) for a finite segment of ribbon cut from a semi-infinite sheet with residual stress as in Fig. 3.

Fig. 5. Shadow Moiré interferogram and in-plane residual stress component σ_{xx} for EFG sheet grown at 1 cm/min.

Fig. 6. Shadow Moiré interferogram and in-plane residual stress component σ_{xx} for EFG sheet grown at 2 cm/min.

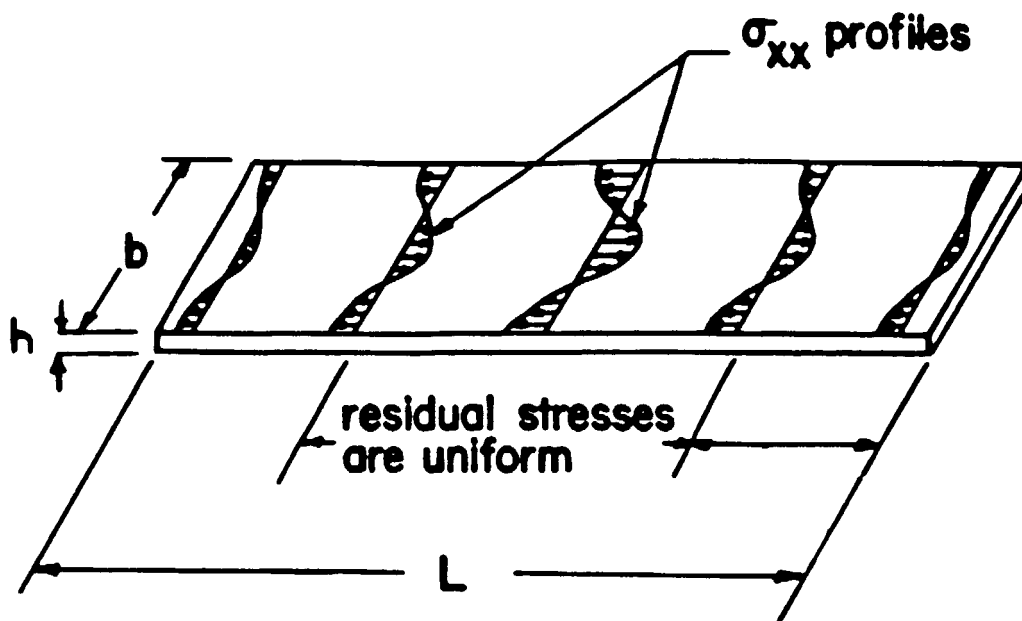Fig. 7. Residual stress distribution in quadrant of 5 x 10 cm^2 blank of EFG sheet grown at 2 cm/min.

Figure 1

Figure 2

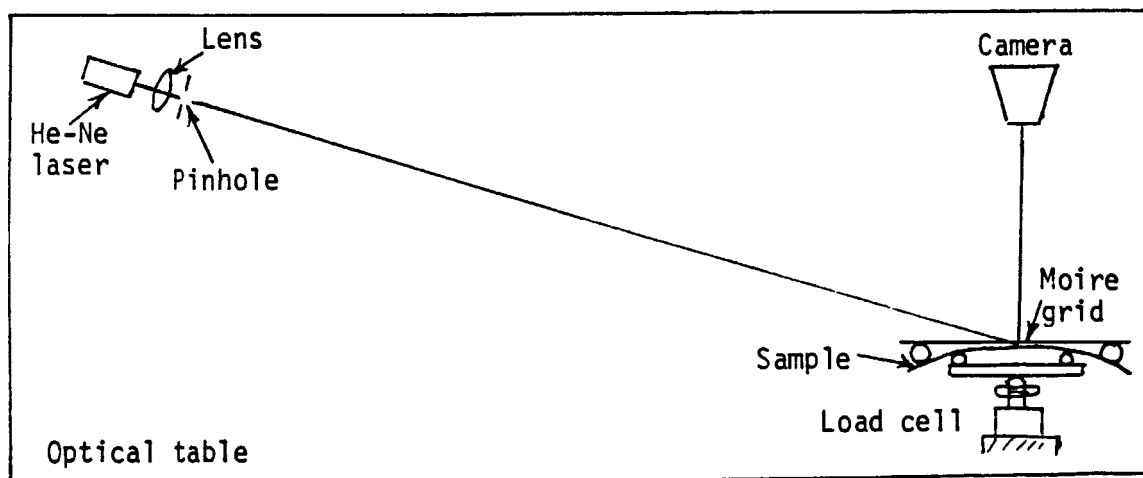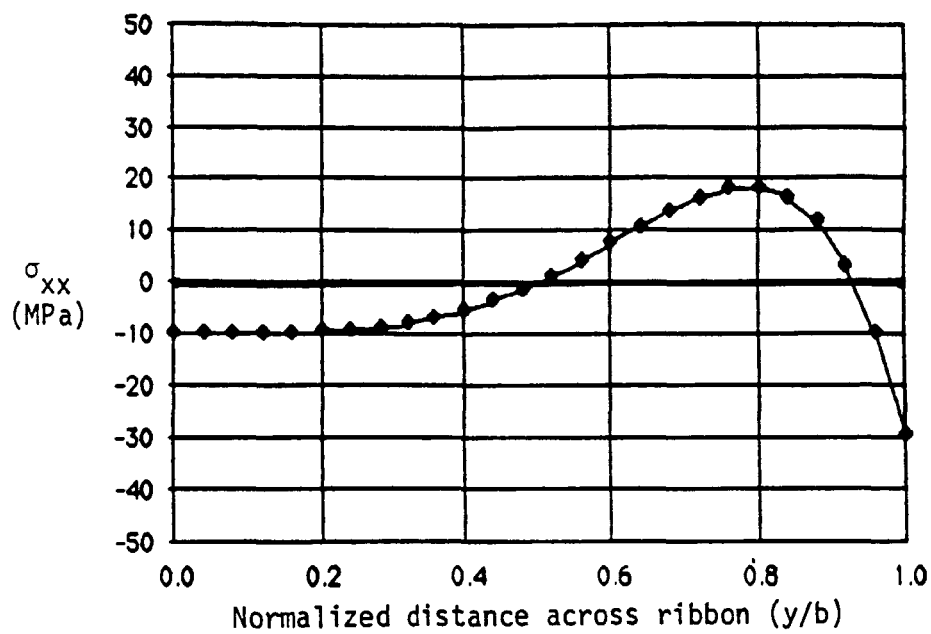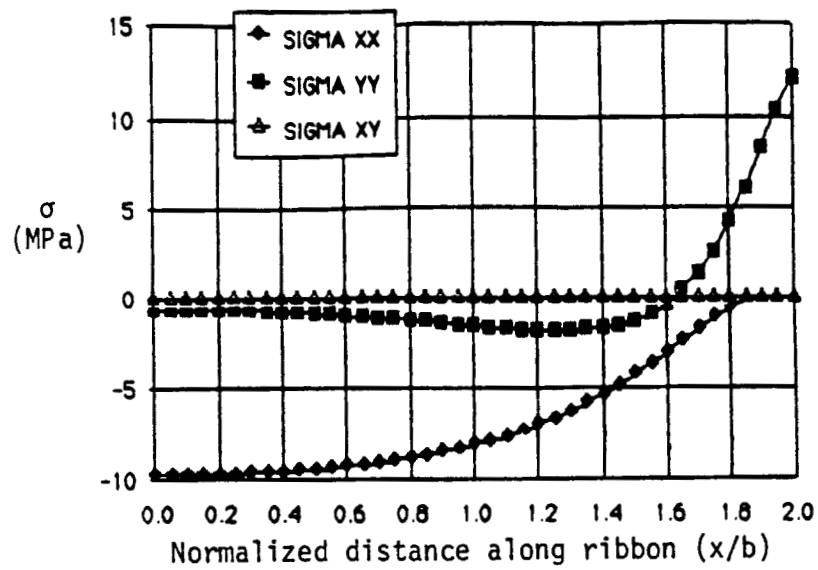Figure 3

Figure 4(a)

Figure 4(b)

Figure 5

69

Figure 6

RESIDUAL STRESS (MPA)

10

5

0

-5

-10

Y

2

1.5

1

0.5

0

X

0.5

1

1.5

2

2.5
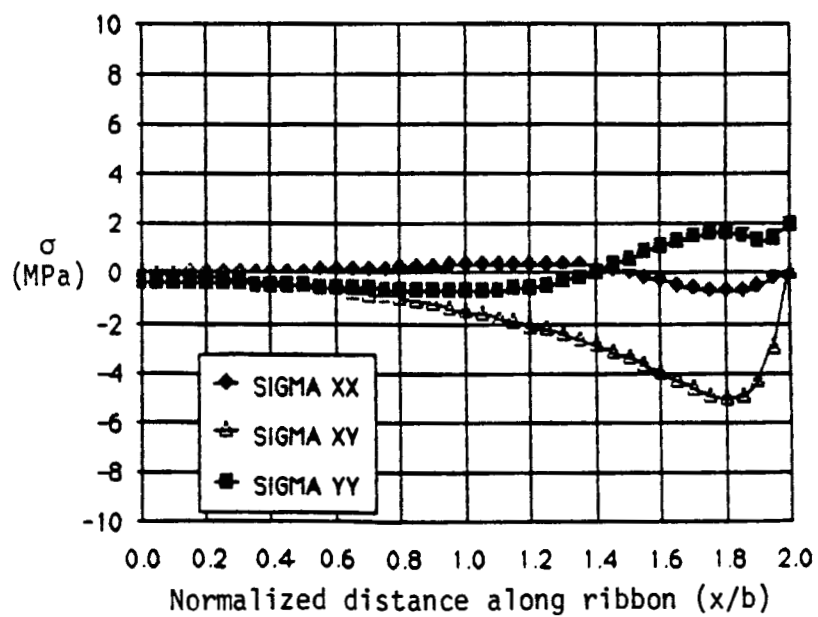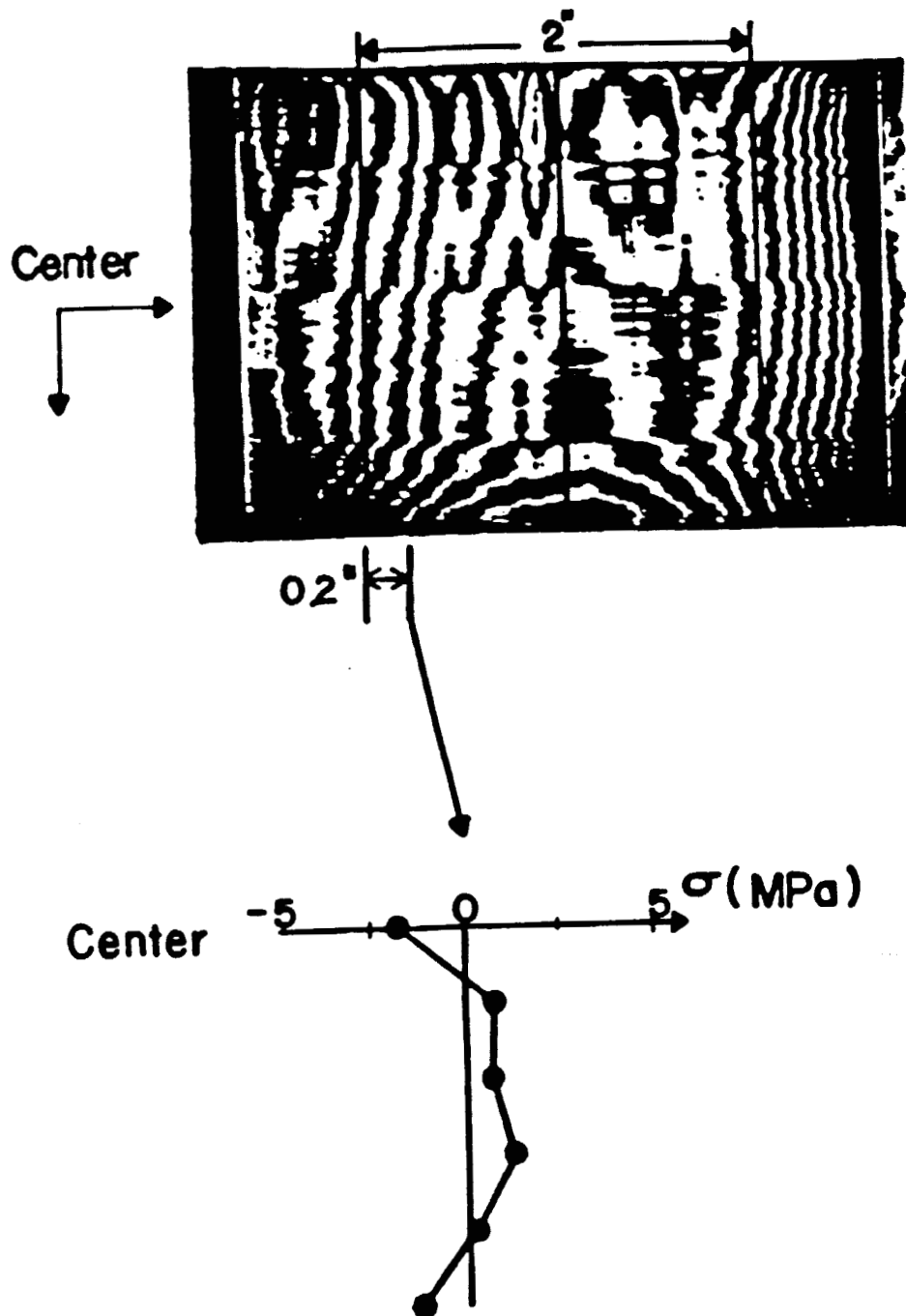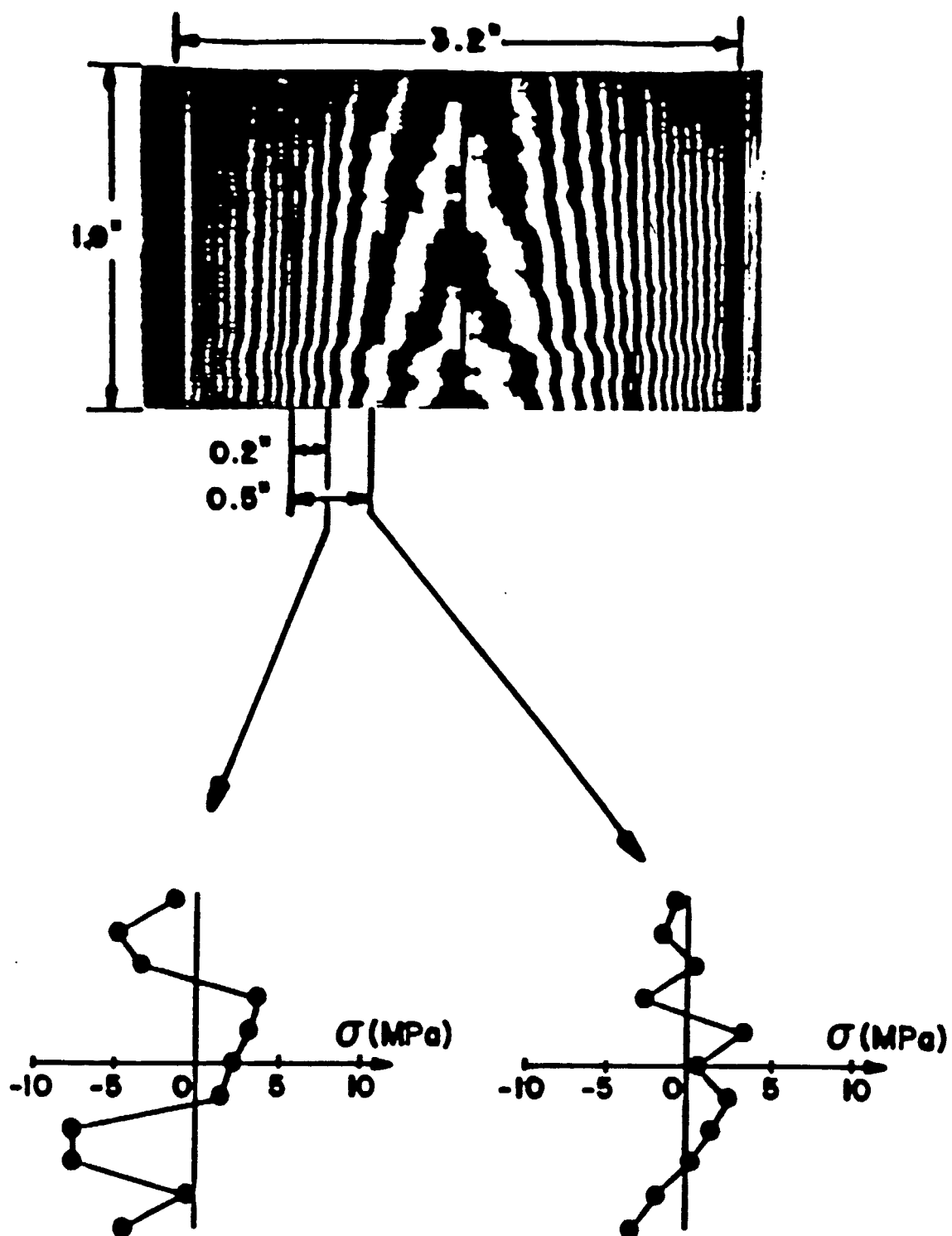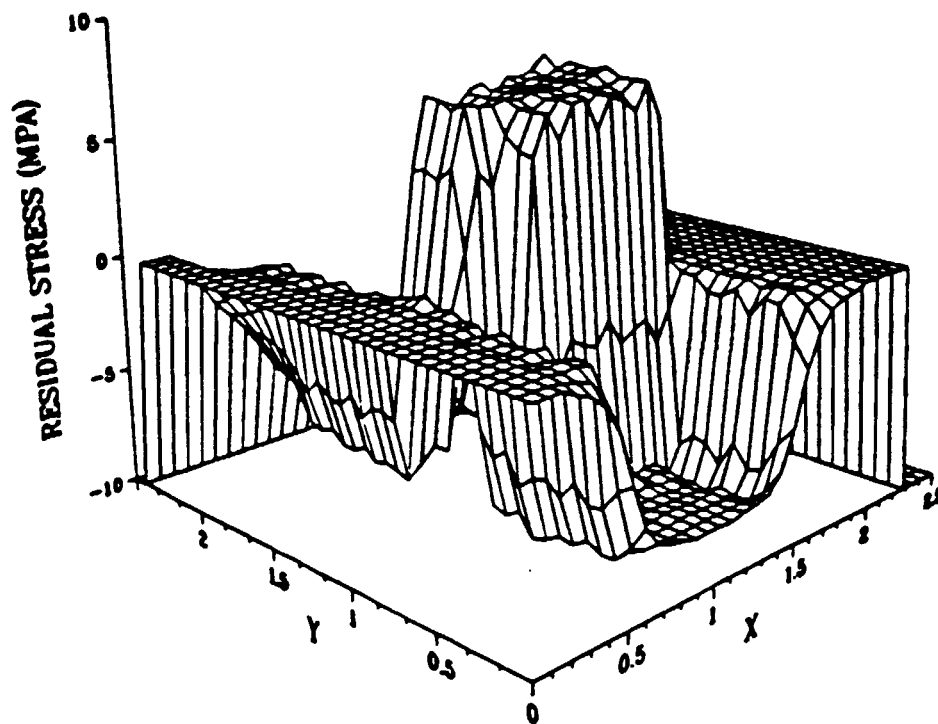
Figure 7

APPENDIX III

Stress Relaxation Measurements
(A.A. Menna, M.P. Brodeur)

The creep response of silicon sheet grown at high speeds has been approximated by a constitutive relationship that is derived for steady-state (secondary) creep, and which does not properly represent plastic deformation during growth. Transient (primary) creep studies in this program have shown that stress relaxation above 1000°C for the initial stages of creep with loading times as short as 10 seconds and dislocation densities less than about $1 \times 10^7/cm^2$ proceeds at rates several orders of magnitude greater than those used for the modeling studies. It is thought that the correct form of a constitutive relationship for creep should reflect stress relaxation at constant strain, which is not measured in either of the above situations. The apparatus that was designed to allow measurement of stress relaxation in silicon above 700°C was suggested by Dr. M. Leipold, and is based on an ASTM 328-78 standard for such testing, adopted for use in the available crystal growth Furnace 17.

A schematic of the equipment that was used is shown in Fig. A1. The sample is loaded in a holder which is in all respects similar to the one used in four-point bending tests. However, provision is made to load the sample and to hold it at a constant deflection while a load cell monitors the stress level in the sample. Thus, the information obtained is in the form of the time rate of change of stress, $\partial\sigma/\partial t$, at constant strain ε. A number of improvements in assembly and experimental technique over the four-point bending apparatus have been incorporated. The all-graphite components are pinned together with movable sections at the base for easy sample setup. Shielded thermocouples measure the temperature at two locations. Argon gas feeds are machined directly into the fixture to ensure proper flow over the sample. A central rod used to measure the deflection by way of a displacement transducer is counterbalanced to prevent additional loading of the sample. Loading is made by the Furnace 17 puller with a load cell measuring load output.

All the samples used in the stress relaxation measurements reported here were (111) surface three inch diameter FZ silicon wafers in the as-received state, that is, with one surface polished (placed up or in compression) and the other rough. The wafers were cut into 5 cm wide and approximately 7.5 cm long rectangles oriented along $\langle 12\bar{3} \rangle$ in the long direction which was then located perpendicular to the bending axis, a $\langle 111 \rangle$ direction. The stresses by which the experimental data are characterized refer to the surface fiber stress (σ_s) and strain (ε_s) given by [6]:
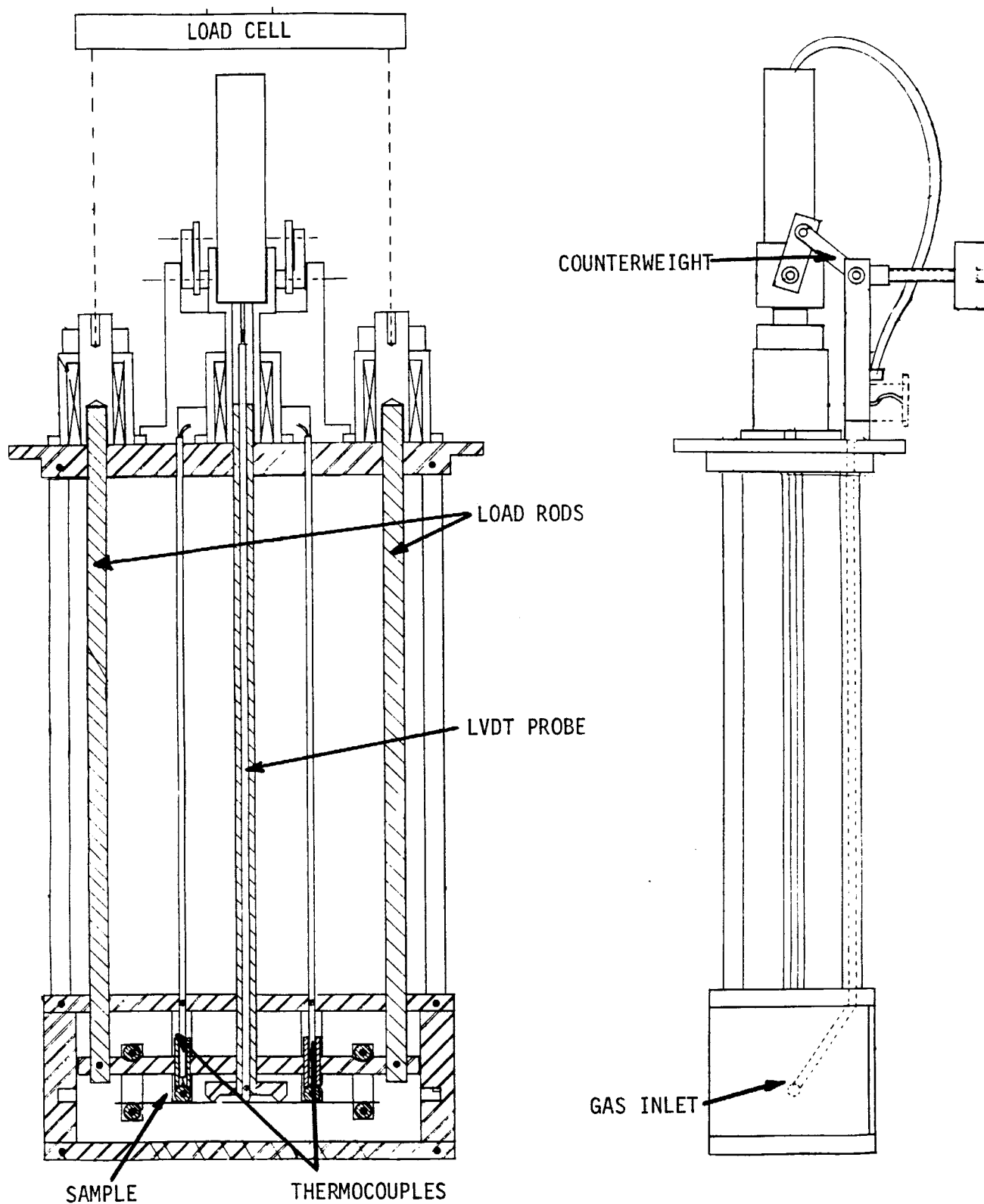
Fig. A1. Stress relaxation fixture, hot zone section.

$$\sigma_s = \pm \frac{6M}{Wt^2}, \quad \varepsilon_s = \pm 4t\delta/L^2$$

where the elastic limit (n = 1) and linear solid representations are used, respectively. The calculated σ_s and ε_s represent the initial loading conditions at time $\tau = 0$, and are reasonable parameters with which to characterize the data. For the samples used, the width W = 4.98 cm, the thickness t = 0.0381 cm, L = 5 cm, and ℓ = 1.25 cm. The moment M = Fℓ, where F is half the applied load on the sample.

The stress and strain parameters appropriate to the data presented in Fig. A2 are given below for the four temperatures at which measurements were taken:

Table A1. Stress/Strain Data for Relaxation Experiments.

| T (°C) | Nominal Values | | | Measured Values | |
	σ_a (MPa)	δ (mm)	ε_a	σ_m (MPa)	ε_m
600	60	1.22	7.4 x 10-4	45	5.6 x 10-4
800	60	1.22	7.4	50	6.3
	90	1.83	11.0	75	9.3
1000	30	0.30	1.9	17	1.0
	60 (2s)	1.22	7.4	60	7.4
	60 (10s)	1.22	7.4	50	6.3
	90	1.83	11.0	70	8.7
1200	30	0.30	1.9	17	1.0
	60	1.22	7.4	35	4.3

The nominal set of values for σ_a and ε_a had to be established for each sample because it was found that it was not a straightforward task to set the reference point of the displacement micrometer to obtain a pre-selected stress and strain. The apparatus and sample expanded in heating up, and this changed the displacement distance considerably from that set at room temperature. The following procedure was therefore adopted. A calibration was made to obtain the applied load/displacement relationship of the apparatus at room temperature. A silicon wafer identical to those used in the bending experiments was used as the test piece. This gave the applied stress (σ_a) and δ values given in Table A1, from which ε_a was calculated. Then the sample was heated up to 600°C where a careful adjustment was made to bring the four-point bending apparatus bars into close contact with the sample and thus adjust for thermal expansion. Then the sample was further heated to the experimental temperature. Some additional thermal adjustments occurred in this subsequent heat-up. These are reflected in the fact that the peak measured stresses (σ_m) in Table A1 differ from σ_a. ε_m was calculated to reflect the change in σ from σ_a to σ_m, using the room temperature curve for the load and displacement relationships. This does not reflect changes in the elastic modulus that may have occurred up to the operating point.
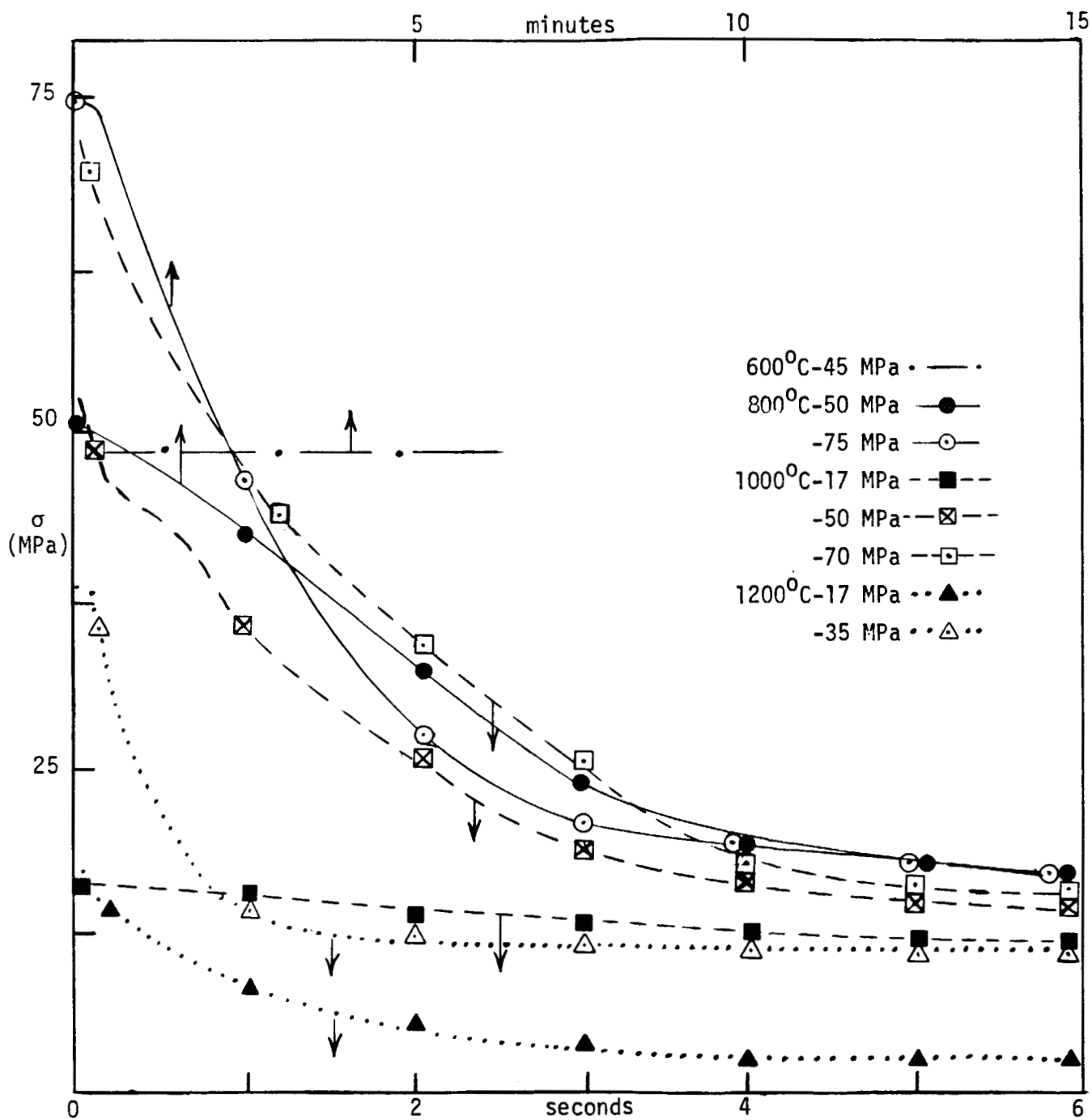
Fig. A2. Stress relaxation data for FZ silicon in the temperature range from 600°C to 1200°C.

A pneumatic loading mechanism was used to bend the sample until it reached the desired displacement, fixed by the micrometer and a mechanical "stop" that stopped the traverse of the load rods at the pre-selected sample displacement. The pneumatic load application mechanism imposed the full displacement and load in a few tenths of a second. The measured stress in Table A1 is the maximum load cell reading recorded at the instant of firing of the pneumatic loader. It varies from about 50 to 100 percent of the nominal setting recorded at 600°C, and indicates that there is considerable adjustment in the apparatus taking place throughout the temperature range up to 1200°C. The lower loads are most severely affected, because of the small displacements involved. It is estimated that displacements can be set to within about 2 mils, or 0.05 mm, corresponding to 50 grams in load. This corresponds to about 5 MPa in stress.

The data of Fig. A2 show some interesting features. The sample stressed at 600°C shows no creep, as expected from earlier results, at these stress levels. The stress relaxation response for the sample stressed with σ_m = 75 MPa at 800°C shows a very unique response. Very little relaxation occurred in the first 25 seconds after loading (there was about a 5 MPa decrease in stress but it is not resolved on the scale shown in Fig. A2), before a rapid relaxation was initiated. Between about 30 seconds and 4 minutes, the stress has relaxed by a factor of about two-thirds (1/e point). In contrast, it takes about 10 minutes to relax to the 1/e point from a stress of 50 MPa at 800°C. The relaxed stress levels for both 800°C loading conditions became the same after about 10 minutes, independent of the displacement. The plastic deformations measured at room temperature after 22 minutes of relaxation were 0.30 mm and 0.50 mm for the cases of the 50 and 75 MPa loads, respectively. This measurement was made for a chord spanning the 2.5 cm distance between the inner pressure bars. The δ value listed in Table A1 is calculated for a chord of twice this distance, in contrast.

The remainder of the data in Fig. A2 at 1000 and 1200°C are taken over much shorter time intervals and are plotted on the time scale of seconds. At 1000°C, significant stress relaxation has appeared already to have taken place within the time resolution of the measurement technique (several tenths of a second), and the maximum stress recorded may not represent the load at zero time. At a stress of 17 MPa, relaxation is relatively slow, and the stress has only changed by about 25 percent (to 13 MPa) after 6 seconds. The load was kept on for 6 minutes in this experiment, at which time the stress had relaxed to about 5 MPa. At the higher stresses of 50 and 70 MPa examined at 1000°C, stress relaxation is very rapid and the 1/e point in stress reduction is reached within about 4 seconds. After 6 seconds, the stress levels remaining for these two cases differed by less than 3 MPa. After a loading time of 5 minutes, the stress level for the initial load of 70 MPa was reduced to about 10 MPa.

The experiments at 1000°C were expanded to get information on dislocation generation rates by removing the load after short times of application of the stress -- 2, 4, and 10 seconds for a starting stress of 50-70 MPa. Cross sections of some samples are shown in Fig. A3, with dislocation counts for samples stressed for 2 seconds and for 5 minutes
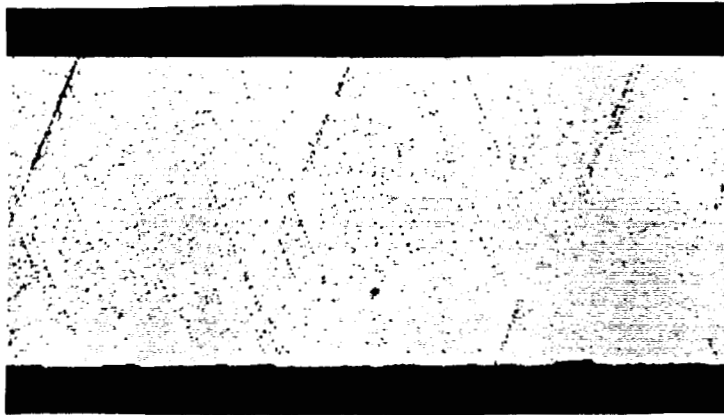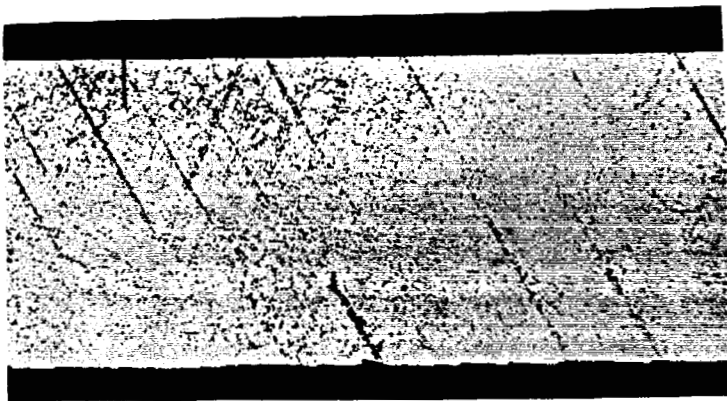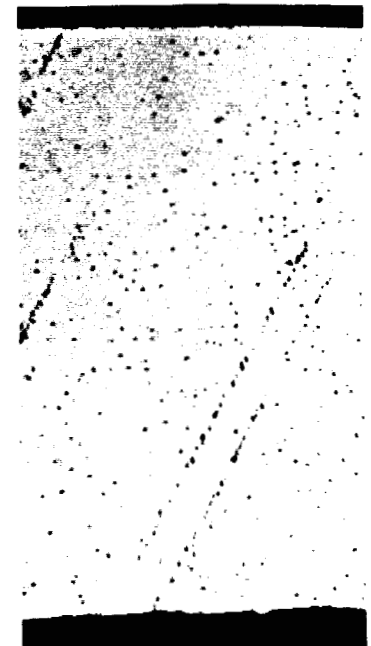
(a)
100X
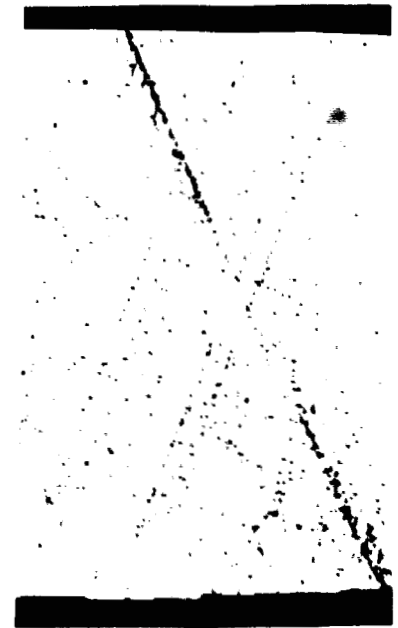
208X
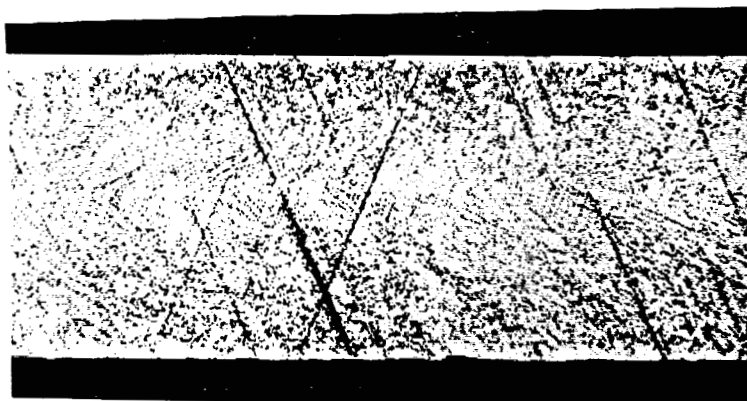
(b)
100X

208X

Fig. A3. FZ silicon cross section micrographs after stressing at 1000°C:
(a) for 2 seconds and 60 MPa, N_d = 3.5 x 10^5/cm^2; (b) for
10 seconds and 50 MPa.

(c)
100X

208X

Fig. A3. FZ silicon cross section micrographs after stressing at 1000°C:
(c) for 5 minutes and 70 MPa, N_d = 1-4 x 10^6/cm^2. Sample
thickness is 0.038 cm, compression surface is down.

at this temperature. Considerable inhomogeneities in dislocation density are in evidence already at very short times of the stress relaxation as the dislocations appear to be clustered on particular slip planes.

The data at 1200°C indicate qualitatively similar stress relaxation effects as at 1000°C, except that at a starting stress of 35 MPa, nearly complete relaxation has occurred already within 1 second of loading.

Techniques by which a constitutive relationship appropriate for stress analysis may be extracted from the new data have been examined in a preliminary study, but no extended analysis has been attempted up to this time. The relaxation time constants characteristic of the various temperatures which have been measured are only representative of those needed for a complete stress analysis of a growing sheet, where a continuous drop in temperature is superimposed on the relaxation phenomenon. More complete data would be needed to derive a detailed representation of the constitutive law. Here, only a few guiding principles for analysis of relaxation phenomena will be mentioned.

Fixed-displacement creep has been examined in detail in the literature [A1]. The constitutive law is often taken to be of the form used for time hardening power law creep:

$$\dot{\varepsilon} = \frac{\dot{\sigma}}{E} + g(t) \, \sigma^n$$

where $g(t)$ is a simple function of time and needs to be deduced from the experimental data. For a beam bent under a stress σ_0 at time $\tau = 0$, the stress at any time τ is then

$$\frac{\sigma(\tau)}{\sigma_0} = [1 + (n - 1)E \int g(t) \, dt \, \sigma_0^{n-1}]^{-1/n-1}$$

where $\tau^* = \sigma_0^{n-1} E \int g(t) \, dt$ is considered as a reduced time, and used as a plotting parameter. Data of the form given in Fig. 2A may then be approximately fit taking τ^* as a multiple of the real time, e.g., with an exponent $n \sim 8{-}10$, at 800°C. It is not clear whether this analysis has any relevance in the case of the present data, and more examination of possible approaches to data reduction is needed.

Reference

A1. J.T. Boyle and J. Spence, _Stress Analysis for Creep_ (Butterworths, London, 1983).